Journal of Biological Physics (2020) 46:253–281
https://doi.org/10.1007/s10867-020-09551-8

ORIGINAL PAPER

Effect of delay in transportation of extracellular glucose into cardiomyocytes under diabetic condition: a study through mathematical model

Phonindra Nath Das[1] · Ajay Kumar[2] · Nandadulal Bairagi[3] · Samrat Chatterjee[4]

Received: 11 November 2019 / Accepted: 26 May 2020 / Published online: 25 June 2020

Abstract

A four-dimensional model was built to mimic the cross-talk among plasma glucose, plasma insulin, intracellular glucose and cytoplasmic calcium of a cardiomyocyte. A time delay was considered to represent the time required for performing various cellular mechanisms between activation of insulin receptor and subsequent glucose entry from extracellular region into intracellular region of a cardiac cell. We analysed the delay-induced model and deciphered conditions for stability and bifurcation. Extensive numerical computations were performed to validate the analytical results and give further insights. Sensitivity study of the system parameters using LHS-PRCC method reveals that some rate parameters, which represent the input of plasma glucose, absorption of glucose by noncardiac cells and insulin production, are sensitive and may cause significant change in the system dynamics. It was observed that the time taken for transportation of extracellular glucose into the cell through GLUT4 plays an important role in maintaining physiological oscillations of the state variables. Parameter recalibration exercise showed that reduced input rate of glucose in the blood plasma or an alteration in transportation delay may be used for therapeutic targets in diabetic-like condition for maintaining normal cardiac function.

Keywords Delay differential equation · Transportation delay · Calcium oscillations · G-I interaction model

✉ Samrat Chatterjee
samrat.chatterjee@thsti.res.in

[1] Department of Mathematics, Memari College, Burdwan, West Bengal, 713146, India

[2] Non-communicable disease group, Translational Health Science and Technology Institute, NCR Biotech Science Cluster, Faridabad 121001, India

[3] Centre for Mathematical Biology and Ecology, Department of Mathematics, Jadavpur University, Kolkata, 700032, India

[4] Complex Analysis Group, Translational Health Science and Technology Institute, NCR Biotech Science Cluster, Faridabad, 121001, India

1 Introduction

Calcium, the ubiquitous second messenger, is essential to the cardiac chamber's contraction and relaxation mechanism, a process known as excitation-contraction (EC) coupling [1]. This second messenger is always in dynamic state and oscillates in the range of 40–180 beats per minute (bpm) for normal cardiac cells. Any deviation suggests an unhealthy state [2, 3]. Core calcium dynamics in cardiomyocytes are primarily subject to the membrane's electrical activity that operates voltage-gated channels, allowing calcium to enter into the cell, whereas other ATP-driven pumps, exchangers and channels mediate the calcium fluxes among sub-cellular compartments and across the plasma membrane [4]. Electrical bursting causes oscillations in the intracellular calcium concentration and may lead to oscillatory insulin levels in blood plasma due to pulsatile insulin secretion [5–7]. This type of oscillations may be also observed in the model populations due to consideration of delay time in performing various metabolic activities [8–11]. Any abnormality in calcium homeostasis may play a significant role in progression of common cardiovascular disorders, including cardiac arrhythmias and heart failure [12]. EC coupling consumes a significant amount of cellular energy which is primarily compensated by mitochondrial oxidative phosphorylation [13]. Glucose metabolism compensates up to 20% of total energy requirement of a healthy heart. Extracellular glucose is transported into cardiomyocyte through glucose transporters primarily by GLUT4 in adult cardiomyocytes [14] and this process is tightly regulated by circulating insulin levels [15]. Insulin receptors based on the cell surface undergo auto phosphorylation after insulin binding, which initiates a signalling cascade and results in translocation of GLUT4 to the membrane to facilitate glucose uptake by the cell [16]. Thus, insulin stimulation in vivo increases myocardial glucose utilization by 40–60% [17, 18].

Because of its elevated and strictly regulated energy requirements, changes in systemic insulin sensitivity or changes in myocardial insulin action may affect cardiac metabolism and functioning. Diabetes-like condition (insulin resistance) impairs the ability of the heart to adjust with the changing energy demands. For example, insulin resistance affects GLUT4 activity, which sometimes leads to cardiovascular complications [19]. Any deregulation, either in the insulin level or in extracellular/intracellular glucose level or consequent alterations in calcium oscillations, may have insulting effect on cardiac function and hence health of the heart per se [3, 20]. Contractile dysfunction due to reduced Ca^{2+} transients is one of the major causes of diabetic cardiomyopathy and the decreased Ca^{2+} sensitivity is suggested to be glucose dependent [21].

Comprehensive information on the cross-talk among glucose, insulin and calcium to maintain healthy cardiac functioning is very scattered and lacks a conclusive rationale. Researchers have studied the glucose-insulin regulatory system mainly in beta-cells and skeletal muscle cells [22], but comparatively very few studies have been done on cardiomyocytes [14, 15, 23]. The combined effect of the glucose-insulin regulatory mechanism with calcium dynamics is not well addressed in cardiomyocyte. Therefore, it would be interesting to investigate the cross-talk among glucose, insulin and calcium with respect to a cardiomyocyte. In the present study, we propose a four-dimensional delay differential system involving blood plasma glucose, blood plasma insulin, intracellular glucose and cytoplasmic calcium concentrations in cardiomyocyte as state variables and analyse it to obtain conditions for stability and bifurcation. Besides analytical observations, we

did extensive numerical experiments on the proposed model using realistic parameter values. Sensitivity of system parameters was determined using a statistical technique known as LHS-PRCC analysis. The overall objective of this study is to understand the role of glucose transporting delay in cardiomyocyte, especially under diabetic condition. We also explored the possible restoration mechanisms in the case of cardiomyocyte dysfunction under diabetic condition.

2 Construction of mathematical model

Here we propose a mathematical model that captures the vital interaction among plasma glucose, plasma insulin, intracellular glucose and cytoplasmic calcium of a cardiomyocyte. As depicted in Fig. 1, insulin binds to its receptor (IR) on the cardiomyocyte membrane and communicates a signal to the glucose transporter GLUT4 for activation, resulting in uptake of plasma glucose from the outside to the inside of the cell in a concentration-dependent manner [14, 24]. There is also a negative feedback on the plasma levels of insulin depending on the levels of cytoplasmic glucose. Within a cardiomyocyte, a major portion of intracellular glucose is used for energy production in the form of ATP through the cell energy metabolism process. The remaining glucose is stored inside the cell in different forms [25]. ATP thus generated controls cardiomyocyte calcium dynamics through SERCA2a pump of sarcoplasmic reticulum (SR) [26]. We consider for simplicity that calcium flux through SERCA2a pump is dependent on the intracellular glucose concentration. Cytoplasmic calcium dynamics is regulated through L-type calcium channel (LTCC), Na^+/Ca^{2+} exchanger (NCX) and SR. Calcium enters into the cell via LTCC, which then allows RyR2 channels to release more calcium into cytoplasm from SR, known as calcium-induced calcium release (CICR) [27]. After completion of cardiomyocyte contraction, a portion of cytoplasmic calcium goes back into SR through SERCA2a pump and another portion goes to extracellular region via NCX. A physiologically defined calcium concentration therefore plays a crucial

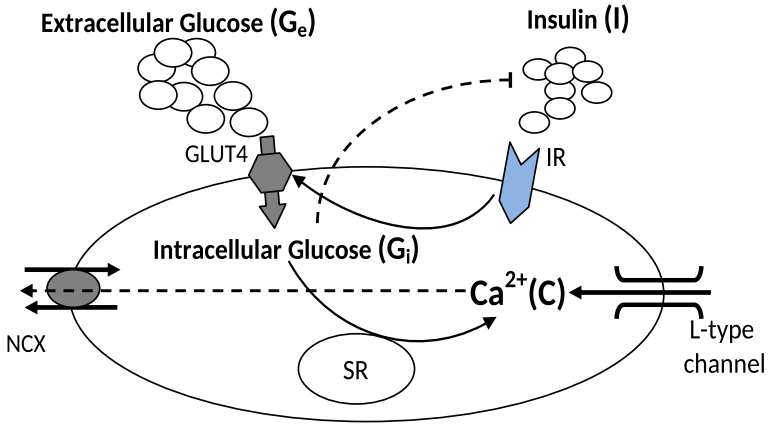

Fig. 1 Schematic diagram of insulin-dependent glucose-calcium interaction in a cardiomyocyte

role in maintaining normal cardiac functioning. Based on this description, we propose the following model:

$$\begin{aligned}
\frac{dG_e}{dt} &= \frac{vG_e}{k_1+G_e} - \frac{rG_eI}{k_2+G_e} - d_1G_e,\\
\frac{dI}{dt} &= b + \frac{eG_eI}{k_3+G_e} - \frac{sIG_i}{k_m+G_i} - d_2I,\\
\frac{dG_i}{dt} &= \frac{rG_eI(t-\tau)}{k_2+G_e} - d_3G_i,\\
\frac{dC}{dt} &= L + \frac{pC^2}{k_4^2+C^2} - \frac{nC^2G_i}{k_5^2+C^2} - d_4C,
\end{aligned} \tag{1}$$

where G_e and I are the concentrations of glucose and insulin in the blood plasma, and G_i and C are the concentrations of intracellular glucose and cytoplasmic calcium of the cardiomyocyte, respectively.

It is observed that glucose input in blood plasma from all sources always maintains a saturation limit [28]. So in the rate equation of extracellular glucose, input of glucose in the blood plasma is represented by the saturated type function $\frac{vG_e}{k_1+G_e}$, where v is the maximum level of plasma glucose and k_1 is the corresponding half-saturation constant. The second term $\frac{rG_eI}{k_2+G_e}$ represents insulin-dependent transport of plasma glucose from outside to inside of the cell with the help of the glucose transporter GLUT4. Here, r is the maximum rate of glucose transportation and k_2 is the corresponding half-saturation constant. The term d_1G_e represents the glucose absorption by cells other than cardiomyocytes, where d_1 is a rate constant.

A baseline insulin is maintained in the blood plasma [29]. Therefore, in the rate equation of insulin, a baseline insulin input in the blood plasma is represented by the constant b. Glucose-dependent insulin secretion from the pancreas in the blood plasma follows a saturated type curve [33] and is represented by the term $\frac{eG_eI}{k_3+G_e}$, where e is the maximum rate of insulin generation and k_3 is the half-saturation constant. It is reported that intracellular glucose (G_i) has a negative feedback on insulin concentration when intracellular glucose reaches some threshold value [30]. This negative feedback effect of intracellular glucose on the plasma insulin has been represented, following [34], by the term $\frac{sIG_i}{k_m+G_i}$, where s is the maximum negative feedback rate and k_m is the corresponding half-saturation constant. A natural degradation of insulin is considered through d_2I, where d_2 is the corresponding degradation rate constant.

In the rate equation of intracellular glucose G_i, the first term represents the transported glucose into the cell by insulin-dependent GLUT4 transporters. GLUT4 is packaged into a specialized compartment and remains static in the absence of insulin. In response to insulin stimulation, GLUT4 is expressed and translocated from intracellular location to the cell membrane, where it allows plasma glucose to enter into the cell [24]. Without considering the intermediate transportation mechanisms in an explicit way, we consider the time τ required for activation of the insulin transporter and subsequent entry of extracellular glucose into the cell. The translocated GLUT4 near the cell membrane at time t, which causes entry of plasma glucose at time t into the cell, is actually the stimulating effect of plasma insulin at time $t-\tau$. This insulin-dependent transportation of glucose, however, saturates as the plasma glucose concentration increases [33]. The first term in the rate equation of intracellular glucose represents such insulin-dependent saturated glucose entry into the cell at a maximum rate r with half-saturation value k_2. A degradation of intracellular glucose is represented by the term d_3G_i, where d_3 is the corresponding rate constant.

In the rate equation of cytoplasmic calcium concentration, a constant calcium input L is considered to represent the calcium influx through L-type channels [31, 32]. The major influx of calcium into the cytoplasm from SR occurs via RyR2 channel and major efflux from the cytoplasm into SR is regulated by SERCA2a pump. RyR2 channel-dependent calcium influx is reported to follow a sigmoid function [35] and considered as $\frac{nC^2G_i}{k_5^2+C^2}$, where n and k_5 are the maximum rate and half-saturation constant respectively. A portion of cytoplasamic calcium goes back to SR through SERCA2a pump and it depends implicitly on the intracellular glucose concentration. Therefore, following [36], we model this efflux by $\frac{nC^2G_i}{k_5^2+C^2}$, where n and k_5 are the maximum rate and half-saturation constant respectively. Change in calcium concentration is relatively fast and quickly reaches to its saturation value [35, 36], and therefore, the Hill constant is assumed to be higher. Another portion of cytoplasmic calcium goes out to extra cellular region through NCX (N^+/Ca^{2+} exchanger) located in the cell membrane. This calcium efflux is assumed to be linear [31, 32] and is denoted by d_4C, where d_4 is a rate constant.

3 Results

3.1 Analytical results

From mathematical point of view, it is important to show that the system (1) has a unique solution which is bounded. This solution should also be non-negative based on the biological constraint that the concentration cannot be negative. We address such issues in Appendix 1. We have obtained conditions for the existence of the interior equilibrium point for the system (1) and its stability conditions in the absence (Appendix 2) and presence of delay (Appendix 3). We have used these conditions in our numerical analysis to understand the nature of the equilibrium point for the considered set of parameter values. We have also observed analytically that delay may cause instability in the system through a Hopf bifurcation provided the length of the delay (τ) exceeds some critical length τ_0 (see Appendix 4). This analytical result is important because it helps us to determine the time length of delay so that the system components oscillate within the physiological range. The direction and stability of the Hopf bifurcation, which are more interesting from mathematical point of view, are presented in Appendix 5.

3.2 Simulation results

3.2.1 Choice of the parameter set and time series analysis

To obtain insight into the system dynamics, extensive simulations were performed. We constructed a parameter set (see Table 1) of which most parameter values were collected from similar studies. Other non-referenced parameters were estimated in such a way that the system components show temporal behaviour within the normal physiological range. For example, the delay parameter τ has been selected so that the system experiences a Hopf bifurcation and the oscillation is maintained in the physiological range. As the glucose absorption rate by noncardiac cells is much higher in comparison with that of cardiac cells, we have chosen $d_1 >> r$. The fasting blood glucose level between 3.9 and 6.1 mM/l is termed as normal; glucose level between 6.1 and 6.9 mM/l is occurs as prediabetic and said to be diabetic if the blood glucose level crosses 6.9 mM/l. Hypoglycemia is occurs if the

Table 1 Description of system parameters with their default values and references

Para.	Definition	Value and unit	Reference
v	Maximum levels of plasma glucose	3.5 mM s^{-1}	[37]
k_1	Half-saturation constant of glucose input	1.5 mM	estimated
r	Insulin-dependent glucose uptake by the cardiac cell	0.0278 mM s^{-1}	[38]
k_2	Half-saturation constant of cell's glucose uptake	10.5 mM	[38]
d_1	Glucose absorption rate by cells other than cardiomyocytes	0.5 s^{-1}	Estimated
b	Basal level of blood insulin	4 pM s^{-1}	[29]
e	Maximum rate of insulin production	36 pM s^{-1}	[37]
k_3	Half-saturation constant of insulin production	30 pM	Estimated
s	Maximum negative feedback of intracellular glucose on insulin	30 mM	Estimated
k_m	Half-saturation constant intracellular glucose's negative feedback on insulin	10 mM	Estimated
d_2	Normal insulin degradation rate	3.5 s^{-1}	Estimated
d_3	Intracellular glucose degradation rate	0.5 s^{-1}	Estimated
L	Calcium input via L-type channels	3.02 μM s^{-1}	[31]
p	Maximum calcium influx rate through RyR2	20 μM s^{-1}	[32]
k_4	Half-aturation constant of RyR2	0.5 μM	[32]
n	Maximum calcium efflux rate via SERCA2a pump	6 μM mM^{-1} s^{-1}	Estimated
k_5	Half-saturation constant of SERCA2a pump	0.1 μM	[32]
d_4	Calcium efflux through cell membrane NCX	10 s^{-1}	[31, 32]

fasting blood glucose level is below 3.9 mM/l [39]. For fasting plasma, normal insulin level should be within 14–174 pM [40]. It is also reported that the amplitude of oscillation of calcium should be more than 0.4 μM [41].

Considering the parameter values as in Table 1, we first verify that $F(G_e^*) = 0$ has a unique positive root (see Appendix 2) and consequently a unique equilibrium point of the system. The leading coefficient and the constant term of $F(G_e^*)$ are respectively -0.0001×10^4 and 2.1613×10^4 and the corresponding positive roots are 600.5195, 5.5141, and 1.5161. Since $G_e^* < g^*(= 5.5000)$ for the feasibility of I^* and G_i^*, so the only feasible root is 1.5161 and consequently the system posses a unique equilibrium point E^*. This equilibrium point E^* will be stable, in the absence of the delay, if it satisfies the conditions of **Theorem 1**. For the parameters given in Table 1, we computed $a_{11} = -0.3261, a_{22} = -0.1041, a_{44} = -8.3409$ and $A_3 + B_2 = 0.4347$, indicating that the conditions of **Theorem 1** are satisfied. Thus, the parameter set given in Table 1 gives a unique equilibrium point E^* which is stable in the absence of delay. Here we want to mention that this parameter set is not unique in satisfying the assumptions of the Theorem 1; rather there exists some non-trivial set of such parameters. For this, we created 500 sets of parameter values by varying each parameter 1.5-fold up and down from its default value and then picked a random set using Latin Hypercube Sampling (LHS). We obtained at least 172 such parameters set which simultaneously satisfy existence and stability conditions of E^*. We have also verified that conditions of **Theorem 3** (see Appendix 4) are satisfied and the critical value of the delay parameter is evaluated as $\tau = \tau_0 = 0.9639$ s. Figure 2 demonstrates that the system is stable for all $\tau < 0.9639$ and oscillatory for $\tau > 0.9639$. Stable

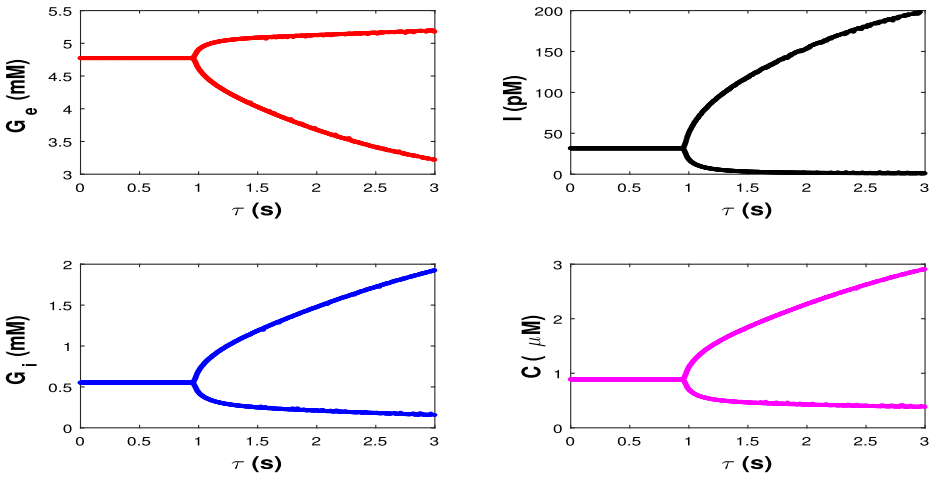

Fig. 2 Bifurcation diagrams of system variables with respect to delay (τ) for the parameter set given in Table 1

time evolutions of each system component for some lower value of delay ($\tau = 0.9 < \tau_0$) are presented in Fig. 3 (in black curve). Each system component shows oscillatory behaviour (see Fig. 3 coloured curve) within the physiological ranges when τ considers the value 1.2 s ($> \tau_0$). For the given parameter set, using **Theorem 4** (see Appendix 5), one can evaluate that $\mu_2 = 17.4876$, $\beta_2 = -3.6864$, and $T_2 = 106.5212$. Since $\mu_2 > 0$ and $\beta_2 < 0$, the Hopf bifurcation is supercritical and the bifurcating periodic solution exists when τ crosses τ_0 from left to right. Also, the bifurcating periodic solution is stable (as $\beta_2 < 0$) and its period is increasing with τ (as $T_2 > 0$). Figure 2 shows that when τ exceeds the critical value τ_0, the system (1) bifurcates from stable focus to stable limit cycle. One can also note that the

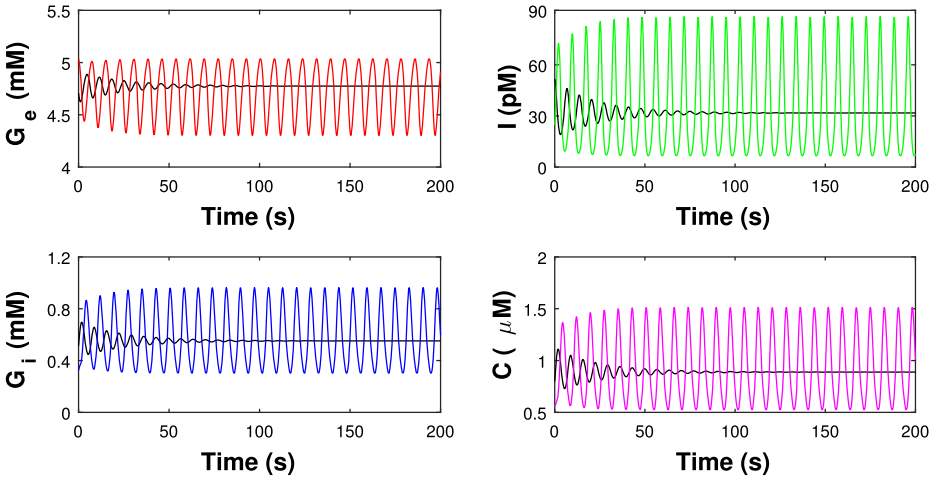

Fig. 3 Simulation time courses show stability (in black curves) of the interior equilibrium point E^* of the system for the parameter set given in Table 1 with $\tau = 0.8$ s ($< \tau_0 = 0.9639$), whereas they show oscillatory behaviour for $\tau = 1.2$ s ($> \tau_0$)

amplitude of the oscillations increases with increasing τ. Lower level of plasma glucose crosses the limit 3.9 mM/l if τ exceeds 1.5 seconds. We, therefore, fix $\tau = 1.2$ seconds as our default value so that plasma glucose oscillates in the normal physiological range.

3.2.2 Global sensitivity analysis

To check the sensitivity of each parameter, we performed the global sensitivity analysis (GSA) using Latin Hypercube Sampling (LHS) and partial rank correlation coefficient (PRCC) sensitivity analysis [42]. Sensitivity of each parameter is plotted in a bar graph (see Fig. 4) and measured in terms of the bar length. A parameter is said to be sensitive with respect to a variable if its PRCC value is greater than $\pm$ 0.3 [43]. One can easily note from Fig. 4 that the parameters v, d_1, e, d_2, d_3 and τ are sensitive parameters for the system (1).

3.2.3 Robustness of parameters

For this analysis we considered the default value of delay ($\tau = 1.2$ s) and then observed the system output (see Table 2) due to variation of each sensitive parameter (both upwards and downwards) while keeping other system parameters fixed. The objective is to find the range of the sensitive parameters for which normal physiological oscillations (PO) of the system variables are maintained.

3.2.4 Two-parameter bifurcation analysis

Two-parameter bifurcation analysis is important because it demonstrates the physiological states of the system component when two sensitive parameters are perturbed simultaneously. Our global sensitivity analysis shows that plasma glucose level (v) is the most sensitive parameter. We therefore observed the variational effect of other sensitive parameters with

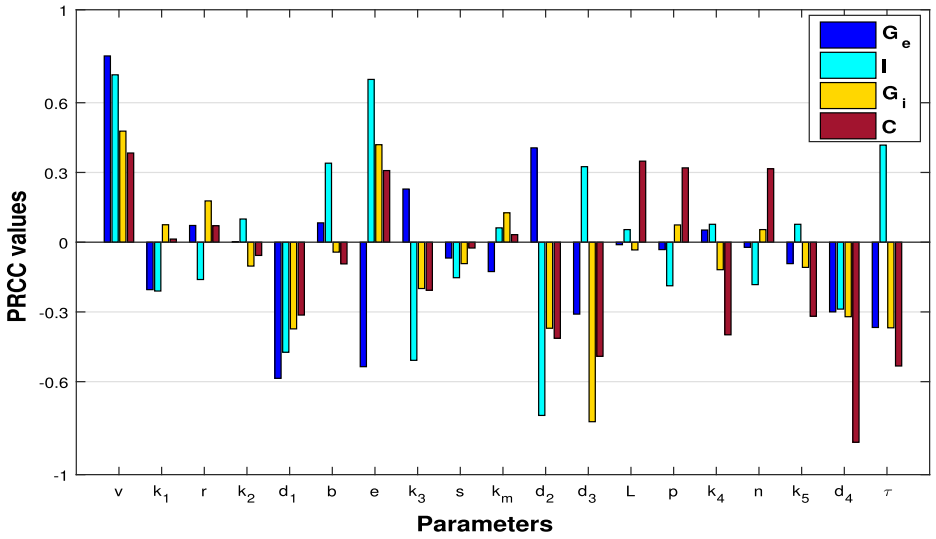

Fig. 4 Parameter sensitivity with the help of PRCC technique. A parameter is assumed to be sensitive if PRCC is greater than $\pm$ 3. Here v, d_1, e, d_2, d_3 and τ are sensitive parameters

Table 2 Robustness of sensitive parameters with respect to normal physiological oscillations of system components

Parameters	Range for PO	Stability range	NPO
v	$3.5 \leq v < 4.05$	$v \leq 3.45$	$3.45 < v < 3.5$, $v \geq 4.05$
d_1	$0.425 < d_1 \leq 0.5$	$d_1 > 0.5$	$d_1 \leq 0.425$
e	$36 \leq e < 42.2$	$e < 36$	$e \geq 42.2$
d_2	$2.7 < d_2 \leq 3.5$	$d_2 > 3.5$	$d_2 \leq 2.7$
d_3	$0.5 \leq d_3 < 0.78$	$d_3 < 0.45$	$0.45 \leq d_3 < 0.5$, $d_3 \geq 0.78$

Here we kept delay at its default value $\tau = 1.2$ s. System oscillations were considered normal if plasma levels of glucose and insulin remain below 6.1 mM/l and 174 pM, respectively, and calcium level exceeds 0.4 μM

respect to v (see Fig. 5). We used green colour to represent the physiological oscillations (PO) of the system components. The non-physiological oscillations (NPO) and the stable behaviour (no oscillations) are represented by the red colour. The narrow range of PO

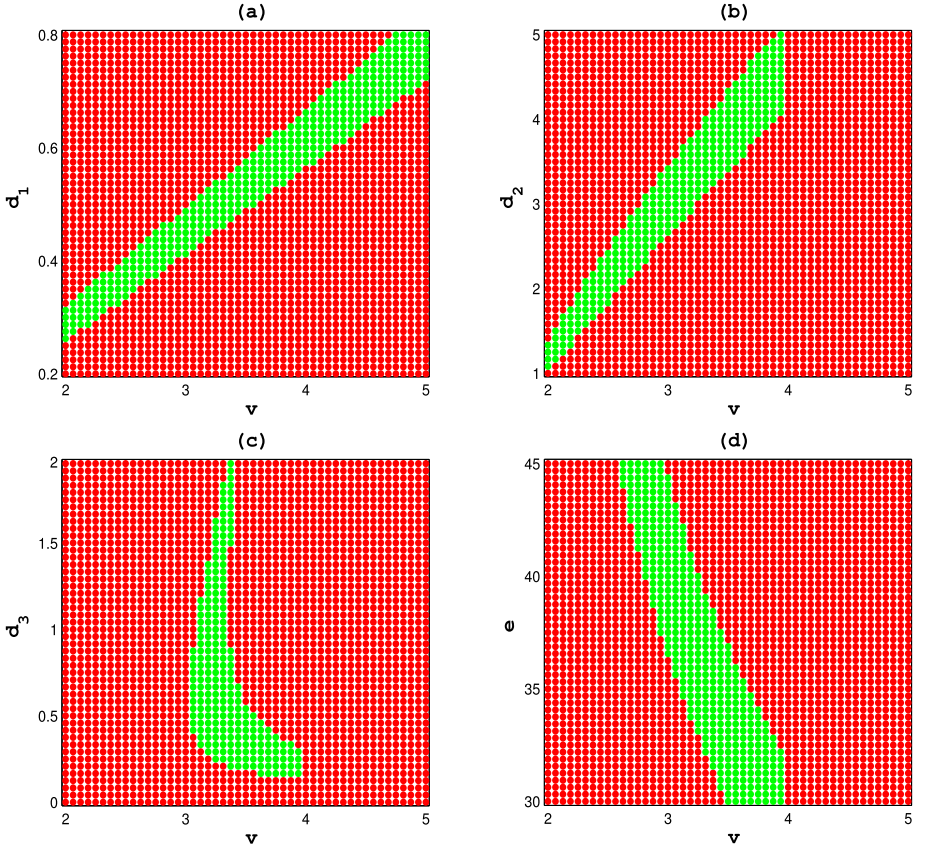

Fig. 5 Two-parameter bifurcation analysis for fixed $\tau = 1.2$ s: **a** v vs d_1, **b** v vs d_2, **c** v vs d_3 and **d** v vs e. In the green colour region, system components oscillate in physiological range and in red coloured region either they become stable or oscillate beyond the physiological range. Bounds for fasting PO range are considered as follows: glucose level between 3.9 and 6.1 mM/l, insulin between 14 and 174 pM and calcium level above 0.4 μM

indicates that plasma glucose level (v) is highly sensitive for maintaining normal oscillations. Figure 5 a and b show that plasma glucose level (v) has a linear relationship with glucose absorption rate by cells other than cardiomyocytes (d_1) and insulin degradation rate (d_2). It is observed that the existence of PO depends mainly on glucose input rate (v) in comparison with intracellular glucose degradation rate (d_3) or insulin production rate (e) (Fig. 5c, d). Delay τ is another sensitive parameter that plays a crucial role in normal Ca^{2+} oscillations in cardiomyocyte. To maintain PO, the length of delay should be smaller when glucose input rate (v), intracellular glucose degradation rate (d_3) and insulin production rate (e) are high (see Fig. 6). The interdependency is opposite in the case of other pairs, viz. (τ, d_1) and (τ, d_2). Out of these, the sensitive pair (τ, e) has the largest PO regime and could be used as therapeutic target in maintaining system's normalcy. Similar direct relationship is observed when insulin production rate (e) is varied along with d_1, d_2 and inverse relationship is observed when it is varied with d_3 (see Fig. 7).

3.2.5 Parameter recalibration analysis

Our GSA analysis did not identify the insulin-dependent glucose uptake rate (r) of cardiomyocyte as a sensitive parameter but it has a significant impact on the progression of diabetic cardiomyocytes. In the case of insulin-resistant diabetic condition, transporta of plasma glucose into cardiomyocytes is hampered, causing a perturbation in the parameter r. We therefore presented a detailed exploration for this parameter and observed that both suppression and over-expression of r lead towards diminished calcium oscillations or violate the upper limits of both extracellular glucose level and insulin level. To demonstrate this we increased and decreased r by 2-, 3-, 4- and 5-fold. It was noticed that for a 2-fold reduction the system behaves normally and there is no need to recalibrate any parameter,

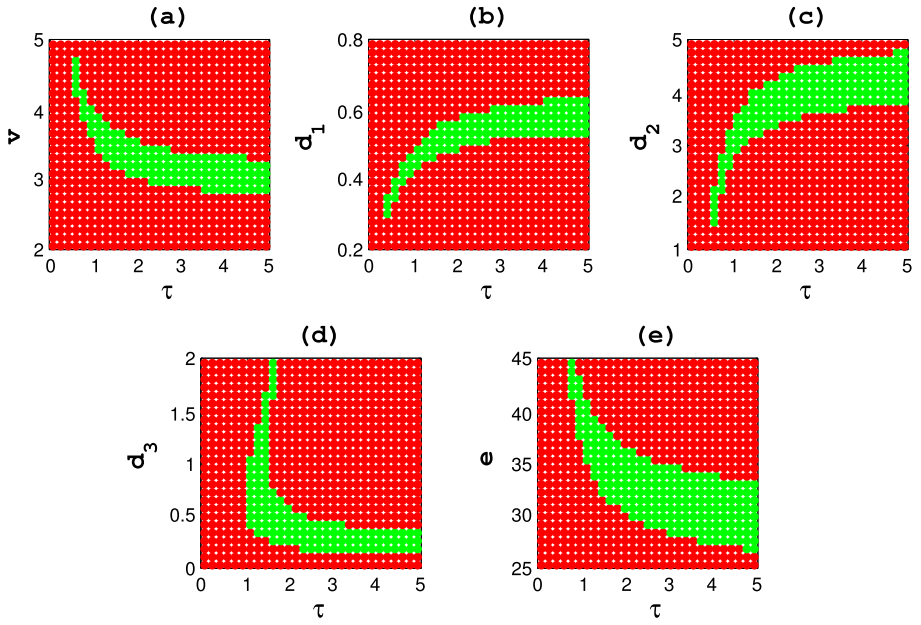

Fig. 6 Two-parametric bifurcation analysis with delay versus other sensitive parameters. Colour interpretation is same as in Fig. 5

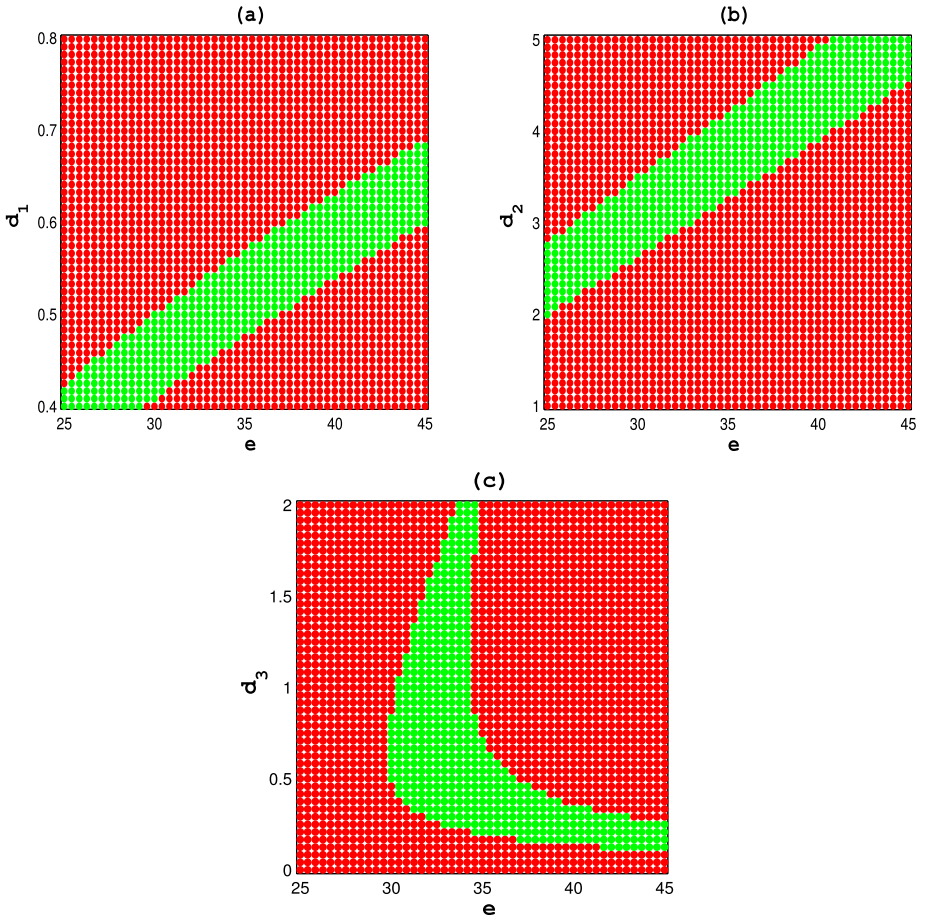

Fig. 7 Two-parametric bifurcation analysis for fixed $\tau = 1.2$ s: **a** e vs d_1, **b** e vs d_2 and **c** e vs d_3. Different coloured regions have the same meaning as in Fig. 5

but any higher fold change in r creates dysfunction. We observed that most of the sensitive parameters can restore normalcy when r is increased, but fail to do so when r is decreased. For example, one can maintain normalcy even for a5-fold increase in r by regulating the parameter d_1, but this is not possible when r is reduced beyond 3-fold. A complete result showing the role of different sensitive parameters on restoring normalcy due to variation in r is given in Table 3, and Fig. 8 shows a visualization of these recalibrations.

Two parameters, τ and d_1, are also important as far as the diabetic patient is concerned because glucose absorption by noncardiac cells may decrease significantly and the time required for insulin-dependent glucose transport may increase in diabetic cardiomyocytes. Therefore, a similar recalibration exercise was done considering τ (Fig. 9) and d_1 (Fig. 10) as target parameters. Figure 9 shows that v, d_1, e and d_2 are the key parameters to restore PO from NPO state due to variation in τ. Though d_3 can restore the system but it cannot be considered as a good recalibrating parameter as it requires high fold change for restoring the system. In the other case, there is only three parameters (v, τ and r) that can recalibrate the system when d_1 is perturbed (see Fig. 10). However, v and τ are better parameters

Table 3 Restoration of normal calcium oscillations and plasma glucose & insulin levels by recalibrating sensitive parameters. Here we kept delay at $\tau = 1.2$ s fixed

Para.	$\frac{r}{5}$	$\frac{r}{4}$	$\frac{r}{3}$	$\frac{r}{2}$	$2r$	$3r$	$4r$	$5r$
τ	N.W.	N.W.	1.156f.d.	N.R.	1.250f.i.	1.400f.i.	1.620f.i.	1.830f.i.
v	N.W.	N.W.	1.035f.d.	N.R.	1.053f.i.	1.100f.i.	1.143f.i.	1.183f.i.
d_1	N.W.	N.W.	1.037f.i.	N.R.	1.057f.d.	1.110f.d.	1.159f.d.	1.207f.d.
e	N.W.	1.066f.d.	1.056f.d.	N.R.	1.068f.i.	1.128f.i.	1.185f.i.	1.241f.i.
d_2	N.W.	1.09f.i.	1.059f.i.	N.R.	1.102f.d.	1.205f.d.	1.315f.d.	1.435f.d.
d_3	2.33f.d.	1.980f.d.	1.540f.d.	N.R.	N.W.	N.W.	N.W.	N.W.

G_e and I levels were maintained bellow 6.1 mM and 174 pM, respectively. Amplitude of Ca^{2+} oscillation was maintained above 0.4 μM. Here N.W.: not working, means that variation in corresponding parameter is unable to restore normal G_e and I levels and normal amplitude of Ca^{2+} oscillations. N.R.: variation not required, f.d.: fold decrease and f.i.: fold increase

for recalibration process compared with r as they need little variation to restore system normalcy.

4 Discussion

It is very common that diabetic patients are more cardiovascular disease prone. To maintain a healthy cardiac function, systematic plasma glucose transport into cardiomyocytes and in other cells is essential. Calcium is a key element to maintain physiological oscillations (PO) in cardiomyocytes, whereas glucose transportation is maintained by insulin, its receptors and other glucose transporters, like GLUT4. In the transport mechanism, a delay can be crucial to maintaining normal cardiac function. Here we proposed a four-dimensional delay-induced model to understand the complex interaction among plasma

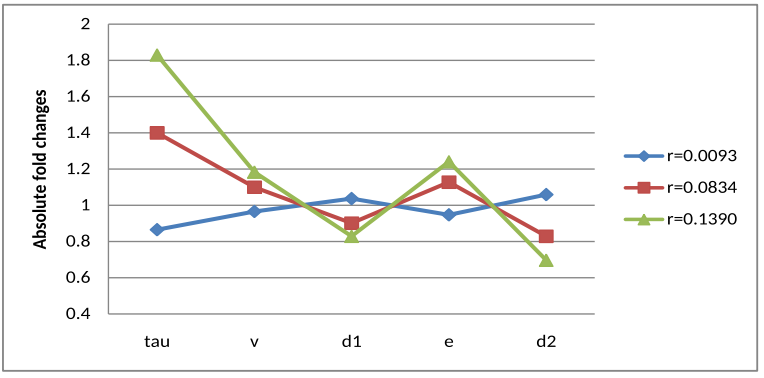

Fig. 8 This figure depicts required fold change in each sensitive parameter to restore normal system (glucose level $G_e < 6.1$ mM, insulin level $I < 174$ pM and Ca^{2+} oscillations amplitude above 0.4 μM) due to an increase or decrease in insulin-dependent glucose uptake rate (r) from its default value $r = 0.0278$. For example, v needs to be increased by 1.14- and 1.183-fold to restore system for the values of $r = 0.1112$ and 0.139, respectively. Parameters were kept fixed as in Table 1 with $\tau = 1.2$ s while other parameters were varied

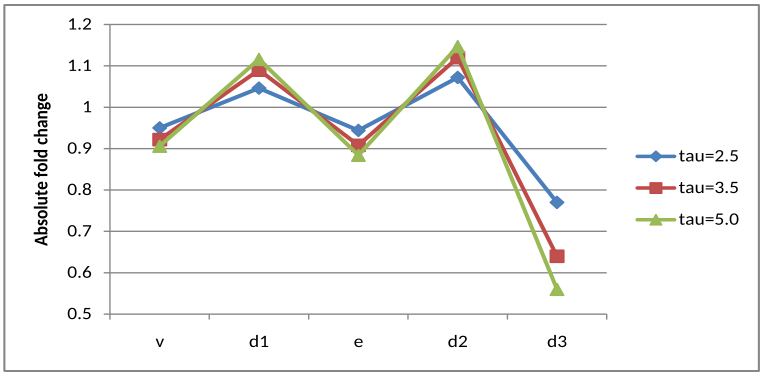

Fig. 9 It depicts required fold change in each sensitive parameter to restore normalcy in the system dynamics due to an increase in the time delay (τ) from its critical value $\tau = 0.9639$ s. For example, v needs to be decreased by 0.95-, 0.92- and 0.90-fold to restore system's normalcy for higher values of $\tau = 2.5$, 3.5 and 5, respectively. Parameters are as in Table 1

glucose, plasma insulin, intracellular glucose and cytoplasmic calcium of a cardiomyocyte under different parametric perturbations. We looked for situations that would help to maintain calcium oscillations of cardiac cells in physiological range along with normal blood glucose and insulin concentrations. A set of conditions was prescribed for the existence of a Hopf bifurcation, leading to periodic oscillations of the system around its interior equilibrium point. We then constructed a parameter set so that blood glucose and insulin remain in normal range and the amplitude of intracellular calcium oscillation is also maintained. It was observed that the system exhibits periodic solutions about the interior equilibrium point if the transport delay τ exceeds some critical value τ_0. However, if τ_0 becomes very high due to some irregularities in the normal process, like in case of delayed phosphorylation or delayed response of insulin receptor for some metabolic reasons, then the system oscillates beyond the physiological range. This means that τ_0 plays a crucial role in maintaining

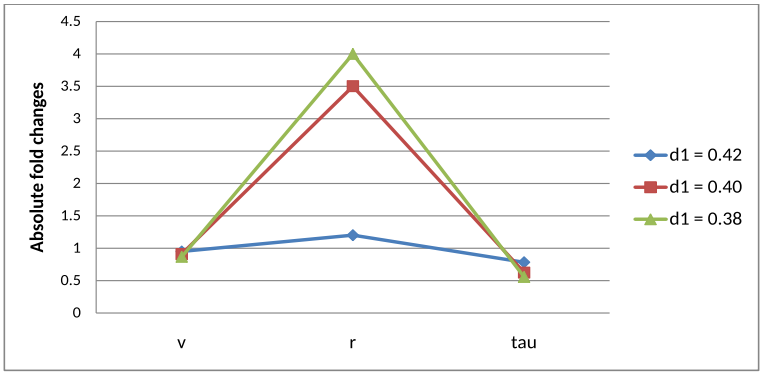

Fig. 10 This figure depicts required fold change in the parameters v, r and τ to restore normal system dynamics due to decreased glucose absorption rate (d_1) in noncardiac cells from its default value $d_1 = 0.5$. For example, v needs to be decreased by 0.94-, 0.90- and 0.86-fold to restore system's normalcy for the lower values of $d_1 = 0.42, 0.40, 0.38$, respectively; whereas r needs multiple fold change for such control. Parameters are as in Table 1 with $\tau = 1.2$ s

physiological range of the state variables and suggests that the length of delay should be maintained within a definite range. Through global sensitivity analysis (GSA), we obtained a set of six sensitive parameters including τ and then performed a robustness analysis to find their ranges satisfying PO. We observed that each sensitive parameter has a finite range for which the system shows PO and beyond which the system shows either stability or non-physiological oscillations (NPO). Sensitive parameters having smaller range for PO (see Table 2) are more important because a small perturbation in these parameters may have a significant effect on the entire system. From this point of view, the parameters v, d_1 and d_3 were considered to be more important. Our sensitivity analysis (see Fig. 4) demonstrated that glucose input rate in the bloodstream v is the most sensitive parameter and directly influences all the state variables. We observed that increased level of glucose, as in the case of diabetic condition, caused an adverse effect on cardiac functioning by diminishing the calcium oscillations. We found a range of v in which the system functioned well. Our global sensitivity analysis also revealed insulin production rate (e), its degradation rate (d_2) and glucose absorption rate (d_1) by noncardiac cells as sensitive parameters. Plasma glucose enters into the cell with the help of insulin to meet the energy requirement of the cell. Furthermore, our robustness analysis showed that any large perturbation in these sensitive parameters could lead to irregular calcium oscillations in cardiac cells. A two-parameter bifurcation analysis was performed on the selected parameters to observe their simultaneous effect on the system dynamics. It is observed that the glucose-dependent insulin production rate had a linear relationship with the degradation rate of plasma glucose and plasma insulin; while it had an inverse relation with intracellular glucose degradation rate. Thus, intracellular glucose degradation rate (d_3) seemed to be an important player in deciding the calcium dynamics within a cardiomyocyte. Besides these two important factors, the main focus of the present study was to mimic diabetic condition leading to change in calcium oscillations, causing cardiac dysfunction. We achieved this in our model by changing parameters related to insulin-dependent glucose uptake rate r and glucose transport delay τ.

4.1 Insulin-dependent glucose uptake by the cell

Insulin-induced GLUT4 translocation regulates glucose uptake in cardiomyocytes. The requirement of glucose for heart function is readily apparent in situations of metabolic stress. Our analysis found insulin-dependent glucose uptake by a cardiomyocyte (r) to be directly proportional to the rate of insulin production (e) and the time taken for glucose uptake (τ), but was inversely proportional to the glucose absorption rate by cells other than cardiomyocytes (d_1). Insulin-dependent glucose uptake via the GLUT4 transporter diminishes during diabetes. Therefore, to mimic a similar scenario, we gradually decreased the value of r. Consequently, a shift in calcium oscillations was observed from physiological range (PO) to non-physiological range (NPO). To restore PO for calcium, parametric recalibration of all parameters except r was done but the possibility of restoration decreased with the reduction in r. As is evident from Table 3, a negligible effect on calcium oscillations was seen when r was halved. However, if r was reduced 3 times, calcium oscillations drifted into NPO. PO could be restored by recalibrating most of the parameters including τ, v, d_1, e, d_2 and d_3. However, further reduction in r by 4 times limited the number of parameters (viz. e, d_2 and d_3) that could restore calcium PO. d_3 was the only parameter which was robust enough to restore calcium PO subsequent to 5-fold reduction in r. No further restoration was possible for larger reduction in the value of r. Hence, decrease in insulin production rate, or increase in insulin degradation rate, or decrease in intracellular degradation rate was revealed as possible and robust strategies to restore calcium PO in a diabetes-like scenario.

4.2 Role of glucose transportation time inside the cell on calcium oscillation

Our GSA identified time delay τ as a sensitive parameter influencing all variables. Time delay refers to the delay in glucose uptake as a result of either faulty IR signalling or delayed GLUT4 translocation. Fold change required for each sensitive parameter to restore system to its normal state is depicted in Fig. 9. Bifurcation analysis revealed that it was important to maintain a minimum τ in order to keep the Ca^{2+} oscillations in the PO range. For a particular value $\tau = 1.2$, a range of different sensitive parameters was identified during which the system maintained POs. Parametric recalibration revealed that τ could be used as a therapeutic strategy in maintaining normal cardiac function in a diabetes-like condition. Through two-dimensional bifurcation analysis we estimated the range of other sensitive parameters against the delay in GLUT4 transportation for maintaining PO. All these observations show that τ plays a significant role in maintaining calcium oscillations in cardiomyocytes. Our observation find supports from published papers [44, 45]. The role of insulin-sensitive GLUT4 in calcium homeostasis was studied in the heart of mouse models [44]. The authors demonstrated that GLUT4 deficiency significantly altered calcium homeostasis in cardiomyocytes. Similarly, the effect of insulin on calcium homeostasis was demonstrated in obese mice by another group from Sweden [45]. The investigators characterized the effect of insulin on calcium homeostasis and demonstrated that insulin enhanced electrically evoked calcium release from obese cells.

4.3 Role of glucose absorption rate by cells other than cardiomyocytes

In diabetic condition, cells other than cardiomyocytes experience disruption in glucose uptake. Our analysis found glucose absorption rate parameter (d_1) for noncardiac cells as a critical parameter which has inverse relationship with all state variables (see Fig. 4). From robustness analysis (Table 2), we found a narrow range of d_1 where the system maintains its PO. It is very interesting to see how this parameter response in diabetic situation due to less consumption of glucose by noncardiac cells. It is observed that if the glucose absorption rate by noncardiac cells is successively reduced form its default value 0.5, then multiple fold change in the parameter value r is required to restore the system's normalcy, implying that r is not a good controller. On the contrary, a small change in the plasma glucose input rate (v) brings normalcy to the system, indicating that v is a good controller. Even the delay parameter τ is a better controller than r. Hence in a diabetic-like situation, either reduced input of glucose into blood plasma or a relatively lower transport delay may play an important role in maintaining PO and could be used for therapeutic targets.

5 Conclusion

One of the main aims of the present work is to investigate the role of time delay associated with the transportation of extracellular glucose into the cardiomyocyte through GLUT4. We observed that the uptake rate of extracellular glucose through GLUT4 and the time required for the activities between the insulin receptor and GLUT4 activation plays a vital role in maintaining normal calcium oscillation. The time required to transport glucose from blood plasma to cellular cytoplasm has a possible therapeutic value and its regulation could restore normalcy in the case of diabetes-like conditions. With the importance of the input rate of glucose into the plasma and the insulin production rate, we observed that regulated glucose input into blood plasma is good for normal oscillations of calcium in cardiomyocytes. We

also observed that there are other ways to control physiological oscillations in calcium and glucose by manipulating other parameters but that depends on the time delay associated with the intracellular glucose uptake rate.

Funding information The work is supported by SERB (Govt. of India) under MATRICS Scheme, Ref No. MTR/2018/000791. Research of NB is supported by RUSA 2.0, Jadavpur University, Ref. No.: R-11/743/19.

Compliance with ethical standards

Conflict of interest The authors declare that they have no conflicts of interest.

Informed consent or animal studies Not applicable.

Appendix 1

Existence and uniqueness of solutions

The initial conditions of the delay differential system (1) have the following form:

$$\begin{aligned} G_e(\theta) &= \phi_1(\theta),\ I(\theta) = \phi_2(\theta),\ G_i(\theta) = \phi_3(\theta),\ C(\theta) = \phi_4(\theta), \\ \phi_i(\theta) &\geq 0,\ \theta \in [-\tau, 0],\ \phi_i(0) > 0,\ i = 1, .., 4, \end{aligned} \tag{2}$$

where $(\phi_1(\theta), .., \phi_4(\theta)) \in C([-\tau, 0], \mathbb{R}^4_+)$ and C is the Banach space of continuous functions mapping the interval $[-\tau, 0]$ into $\mathbb{R}^4_+$ with norm $||\phi|| = \sup_{-\tau \leq \theta \leq 0}\{|\phi_1(\theta)|, |\phi_2(\theta)|, |\phi_3(\theta)|, |\phi_4(\theta)|\}$, where $\phi = \{\phi_1(\theta), .., \phi_4(\theta)\}$.

Positivity and boundedness

For biological demand, we need to prove that all solutions of system (1) with initial conditions (2) are defined on $[0, \infty)$ and remain positive for all $t \geq 0$.

To show global existence of solutions it is enough to show that the right-hand side of (1) is globally Lipschitz. The system (1) can be expressed as

$$\frac{dX}{dt} = f(X), \tag{3}$$

where $X = (x_1, x_2, x_3, x_4)^T$ and $f = (f_1, f_2, f_3, f_4)^T$. The function $f : \mathbb{R}^4_+ \to \mathbb{R}^4_+$ possesses the global Lipschitz condition if there exists a Lipschitz constant $M > 0$ such that $|f(x) - f(y)| \leq M|x - y|$ holds for any $x, y \in \mathbb{R}^4_+$.

Following [46], it can be easily proved that

$$|f_1(x) - f_1(y)| \leq M_1|x - y| \tag{4}$$

$$|f_2(x) - f_2(y)| \leq M_2|x - y| \tag{5}$$

$$|f_3(x) - f_3(y)| \leq M_3|x - y| \tag{6}$$

$$|f_4(x) - f_4(y)| \leq M_4|x - y| \tag{7}$$

where $M_1 = d_1 + v + (1 + K_2)r$, $M_2 = d_2 + (1 + K_2)(e + s)$, $M_3 = d_3 + (1 + K_2)r$, and $M_4 = d_4 + p + (1 + K_3)n$. $M_4 = d_4 + p + (1 + k_3)n$, with the assumption that there exists real positive numbers $k_2 and k_3$ such that $|x_2| leq k_2 and |x_3| leq k_3$.

Now, to obtain the global Lipschitz constant for f, we simply choose $M = \sqrt{M_1^2 + M_2^2 + M_3^2 + M_4^2}$ and obtain

$$|f(x) - f(y)| \leq M|x - y|. \tag{8}$$

Therefore, f, and hence the right-hand side of (1), is globally Lipschitz. Thus, the system possesses a unique solution. Again since f is Lipschitz, then it maps non-negative vectors to non-negative vectors, i.e., (1) gives positive invariant solution with the positive initial condition (2).

Next we show that solutions are bounded. From the first equation of system (1), we have

$$\frac{dG_e}{dt} + d_1 G_e \leq v. \tag{9}$$

Thus, following [47], we get

$$\limsup_{t\to\infty} G_e(t) \leq \frac{v}{d_1},$$

implying that $G_e(t)$ is ultimately bounded.

Using the second equation, we get

$$\frac{dI}{dt} + (d_2 - \frac{ev}{k_3 d_1 + v})I \leq b. \tag{10}$$

Assuming $d_2 > \frac{ev}{k_3 d_1 + v}$, we have

$$\limsup_{t\to\infty} I(t) \leq \Lambda,$$

where $\Lambda = \frac{b(k_3 d_1 + v)}{d_1 d_2 k_3 + d_2 v - ev}$. This shows that $I(t)$ is ultimately bounded.

For all $t > t^* + \tau$, where t^* is any non-negative time, we obtain from the third equation

$$\frac{dG_i}{dt} + d_3 G_i \leq r\Lambda. \tag{11}$$

Again one gets $\limsup_{t\to\infty} G_i(t) \leq \frac{r\Lambda}{d_3}$, implying that $G_i(t)$ is ultimately bounded.

Similarly, we obtain

$$\frac{dC}{dt} + d_4 C \leq L + p \implies \limsup_{t\to\infty} C(t) \leq \Pi, \tag{12}$$

where $\Pi = \frac{L+p}{d_4}$, implying that $C(t)$ is ultimately bounded.

Thus, there exists a unique solution, which is positive for $t > 0$ and is ultimately bounded.

Appendix 2

Equilibrium point and its stability

We are interested in the interior equilibrium point of the system (1) denoted by $E^* \equiv (G_e^*,\ I^*,\ G_i^*,\ C^*)$, where $I^* = \frac{G_e^* + k_2}{r}(\frac{v}{G_e^* + k_1} - d_1)$ and $G_i^* = \frac{G_e^*}{d_3}(\frac{v}{G_e^* + k_1} - d_1)$. Note that $I^*,\ G_i^*$ both exist if $G_e^* < g^*$, where $g^* = \frac{v}{d_1} - k_1$. Thus, steady-state concentrations of insulin and plasma glucose are biologically meaningful if plasma glucose concentration is not too high and lies below the critical level g^*.

Steady-state concentration C^* is given by the positive root of the equation

$$H(C^*) = 0, \tag{13}$$

where

$$H(C^*) = d_4C^{*5} + (nG_i^* - L - p)C^{*4} + d_4(k_4^2 + k_5^2)C^{*3} + \{nk_4^2G_i^* - L(k_4^2 + k_5^2) - pk_5^2\}C^{*2} + k_4^2k_5^2C^* - Lk_4^2k_5^2.$$

It is to be noted that $H(0) < 0$ and $H(\infty) > 0$. Thus, there is at least one positive root of the polynomial $H(C^*)$. Further, if $G_i^* \geq \max\left\{\frac{L+p}{n}, \frac{L}{n} + \frac{L+p}{n}\left(\frac{k_5}{k_4}\right)^2\right\}$ holds then, following Descartes' rule, there is an unique root of (13). The steady state concentration G_e^* is given by the positive root of the equation

$$F(G_e^*) = 0, \tag{14}$$

where

$$F(G_e^*) = P_0G_e^{*5} + P_1G_e^{*4} + P_2G_e^{*3} + P_3G_e^{*2} + P_4G_e^* + P_5,$$

and

$$\begin{aligned}
P_0 &= d_1^2(s + d_2 - e),\\
P_1 &= d_1(k_3A_h + B_h - eD_h) + (A_h - ed_1)F_h + d_1br,\\
P_2 &= d_1\{k_3B_h - C_h + eE_h + (k_1 + k_3)br\} + (A_h - ed_1)G_h + brD_h\\
&\quad + (k_3A_h + B_h - eD_h)F_h,\\
P_3 &= d_1(brk_1k_3 - k_3C_h) + (k_3B_h - C_h + eE_h)F_h + (k_3A_h + B_h - eD_h)G_h,\\
&\quad + \{(k_1 + k_3)D_h - E_h\}br,\\
P_4 &= (k_3B_h - C_h + eE_h)G_h - k_3C_hF_h + \{k_1(k_3D_h - E_h) - k_3E_h\}br,\\
P_5 &= k_1k_3k_md_3\{k_2d_2(v - d_1k_1) - k_1k_3br\},\\
A_h &= d_1(s + d_2),\ B_h = (1 + d_2)(d_1k_1 - v) - d_2d_3k_m,\ C_h = k_1k_md_2d_3,\\
D_h &= d_1k_1 - v - d_3k_m,\ E_h = k_1k_md_3,\ F_h = d_1k_1 - v + d_1k_2,\\
G_h &= d_1k_1k_2 - vk_2.
\end{aligned}$$

Equation (14) has at least one positive real root if P_0 and P_5 have opposite signs and it holds if $e - s < d_2 < \frac{k_1br}{k_2(v - d_1k_1)}$, or $e - s > d_2 > \frac{k_1br}{k_2(v - d_1k_1)}$. Thus, the system (1) has at least one interior equilibrium. In the simulations, we show that the parameter set satisfies the second condition for the existence of a positive root and the root is unique.

After linearization around E^*, system (1) can be expressed in matrix form

$$\frac{d}{dt}\begin{pmatrix} G_e(t)\\ I(t)\\ G_i(t)\\ C(t)\end{pmatrix} = M_1\begin{pmatrix} G_e(t)\\ I(t)\\ G_i(t)\\ C(t)\end{pmatrix} + M_2\begin{pmatrix} G_e(t-\tau)\\ I(t-\tau)\\ G_i(t-\tau)\\ C(t-\tau)\end{pmatrix}, \tag{15}$$

where

$$M_1 = \begin{pmatrix} a_{11} & a_{12} & 0 & 0\\ a_{21} & a_{22} & a_{23} & 0\\ a_{31} & 0 & a_{33} & 0\\ 0 & 0 & a_{43} & a_{44}\end{pmatrix},\quad M_2 = \begin{pmatrix} 0 & 0 & 0 & 0\\ 0 & 0 & 0 & 0\\ 0 & a_{32} & 0 & 0\\ 0 & 0 & 0 & 0\end{pmatrix},$$

and $a_{11} = \frac{vk_1}{(k_1+G_e^*)^2} - \frac{rk_2I^*}{(k_2+G_e^*)^2} - d_1$, $a_{12} = -\frac{rG_e^*}{k_2+G_e^*}$, $a_{21} = \frac{ek_3I^*}{(k_3+G_e^*)^2}$, $a_{22} = \frac{eG_e^*}{k_3+G_e^*} - \frac{sG_i^*}{k_m+G_i^*} - d_2$, $a_{23} = -\frac{sk_mI^*}{(k_m+G_i^*)^2}$, $a_{31} = \frac{rk_2I^*}{(k_2+G_e^*)^2}$, $a_{32} = \frac{rG_e^*}{k_2+G_e^*}$, $a_{33} = -d_3$, $a_{43} = -\frac{nC^{*2}}{k_5^2+C^{*2}}$, $a_{44} = \frac{2pk_4^2C^*}{(k_4^2+C^{*2})^2} - \frac{2nk_5^2G_i^*C^*}{(k_5^2+C^{*2})^2} - d_4$.

The characteristic equation around E^* reads

$$(\lambda - a_{44})\{\lambda^3 + A_1\lambda^2 + (A_2 + B_1 e^{-\lambda\tau})\lambda + A_3 + B_2 e^{-\lambda\tau}\} = 0, \tag{16}$$

where

$$\begin{aligned} A_1 &= -(a_{11} + a_{22} + a_{33}), \\ A_2 &= a_{11}a_{22} + a_{11}a_{33} + a_{22}a_{33} - a_{12}a_{21}, \\ A_3 &= a_{12}a_{21}a_{33} - a_{12}a_{23}a_{31} - a_{11}a_{22}a_{33}, \\ B_1 &= -a_{23}a_{32}, \\ B_2 &= a_{11}a_{23}a_{32}. \end{aligned}$$

From (16), we have one real eigenvalue a_{44} and the other eigenvalues are the roots of the equation

$$P(\lambda, \tau) = \lambda^3 + A_1\lambda^2 + (A_2 + B_1 e^{-\lambda\tau})\lambda + A_3 + B_2 e^{-\lambda\tau} = 0. \tag{17}$$

In the absence of delay, (17) reduces to

$$P(\lambda, 0) = \lambda^3 + A_1\lambda^2 + (A_2 + B_1)\lambda + A_3 + B_2 = 0. \tag{18}$$

Assuming $a_{11} < 0$ and $a_{22} < 0$, we have $A_1 > 0$, $A_2 + B_1 > 0$ and $A_1(A_2 + B_1) - (A_3 + B_2) > 0$. Further, if $A_3 + B_2 > 0$ then, following the Routh-Hurwitz criterion, all three roots of the cubic (18) will have negative real parts. Hence we have the following theorem.

Theorem 1 *If a_{11}, a_{22}, a_{44} are negative and $A_3 + B_2$ is positive, then the equilibrium E^* is locally asymptotically stable in the absence of delay.*

Appendix 3

Following [48, 49], one can easily obtain the following results on the distribution of roots of the transcendental equation (17) and stability of E^*.

Lemma 1 *For the transcendental equation (17), all roots with positive real parts of (17) will have the same sum as those of (18) for all τ if $Q_3 \geq 0$ and $Q_1^2 - 3Q_2 \leq 0$, where $Q_1 = A_1^2 - 2A_2$, $Q_2 = A_2^2 - 2A_1A_3 - B_1^2$ and $Q_3 = A_3^2 - B_2^2$.*

Theorem 2 *Assume that Theorem 1 holds with $Q_3 \geq 0$ and $Q_1^2 - 3Q_2 \leq 0$. Then the equilibrium E^* is locally asymptotically stable for all $\tau \geq 0$.*

Appendix 4

We here consider the delay parameter τ as our bifurcation parameter and determine the condition for delay-dependent instability. For this, let $\lambda(\tau) = \eta(\tau) + i\omega(\tau)$ be the eigenvalue of (17) such that for some value of τ, say $\tau = \tau_0$, we have $\eta(\tau_0) = 0$ and $\omega(\tau_0) = \omega_0 \neq 0$ (without loss of generality, we may assume $\omega_0 > 0$).

Following [48], we have

$$\tau_j = \frac{1}{\omega_0}\cos^{-1}\left[\frac{\omega_0 B_1(\omega_0^3 - \omega_0 A_2) + B_2(\omega_0^2 A_1 - A_3)}{\omega_0^2 B_1^2 + B_2^2}\right] + \frac{2j\pi}{\omega_0} \quad j = 0, 1, 2... \tag{19}$$

We have to show that the transversality condition is satisfied, i.e., $\frac{d(Re\lambda)}{d\tau}\Big|_{\tau=\tau_0} > 0$.

Differentiating the cubic (17) with respect to τ, we get

$$(3\lambda^2 + 2A_1\lambda + A_2)\frac{d\lambda}{d\tau} + e^{-\lambda\tau}\{B_1 - \tau(B_1\lambda + B_2)\}\frac{d\lambda}{d\tau} = \lambda(B_1\lambda + B_2)e^{-\lambda\tau}. \tag{20}$$

It gives

$$\begin{aligned}\left(\frac{d\lambda}{d\tau}\right)^{-1} &= \frac{3\lambda^2 + 2A_1\lambda + A_2}{\lambda(B_1\lambda + B_2)e^{-\lambda\tau}} + \frac{B_1}{\lambda(B_1\lambda + B_2)} - \frac{\tau}{\lambda} \\ &= \frac{2\lambda^3 + A_1\lambda^2 - A_3}{-\lambda^2(\lambda^3 + A_1\lambda^2 + A_2\lambda + A_3)} + \frac{B_2}{-\lambda^2(B_1\lambda + B_2)} - \frac{\tau}{\lambda}.\end{aligned}$$

Now we have

$$\begin{aligned}&Sign\left\{\frac{d(Re\lambda)}{d\tau}\right\}_{\lambda=i\omega_0} = Sign\left\{Re\left(\frac{d\lambda}{d\tau}\right)\right\}_{\lambda=i\omega_0} \\ &= Sign\left\{Re\left[\frac{2\lambda^3 + A_1\lambda^2 - A_3}{-\lambda^2(\lambda^3 + A_1\lambda^2 + A_2\lambda + A_3)}\right] + Re\left[\frac{B_2}{-\lambda^2(B_1\lambda + B_2)}\right]\right\}_{\lambda=i\omega_0} \\ &= Sign\left\{Re\left[\frac{-2\omega_0^3 i - A_1\omega_0^2 - A_3}{\omega_0^2(-\omega_0^3 i - A_1\omega_0^2 + A_2\omega_0 i + A_3)}\right] + Re\left[\frac{B_2}{\omega_0^2(B_1\omega_0 i + B_2)}\right]\right\} \\ &= Sign\left\{\frac{2\omega_0^6 + (A_1^2 - 2A_2)\omega_0^4 - A_3^2}{\omega_0^2\{(A_1\omega_0^2 - A_3)^2 + (\omega_0^3 - A_2\omega_0)^2\}} + \frac{B_2^2}{\omega_0^2(B_2^2 + B_1^2\omega_0^2)}\right\} \\ &= \frac{1}{\omega_0^2}Sign\left\{\frac{2\omega_0^6 + (A_1^2 - 2A_2)\omega_0^4 + B_2^2 - A_3^2}{B_2^2 + B_1^2\omega_0^2}\right\} \\ &= \frac{1}{\omega_0^2}Sign\left\{\frac{H(\mu)}{B_2^2 + B_1^2\omega_0^2}\right\},\end{aligned} \tag{21}$$

where $H(\mu) = 2\mu^3 + (A_1^2 - 2A_2)\mu^2 + B_2^2 - A_3^2$ is evaluated at $\omega_0^2 = \mu$. Differentiating $H(\mu)$ with respect to μ, we have

$$\frac{dH(\mu)}{d\mu} = 6\mu^2 + 2(A_1^2 - 2A_2)\mu. \tag{22}$$

Two roots of $\frac{dH(\mu)}{d\mu} = 0$ can be written as

$$\mu_1 = 0, \quad \mu_2 = -\frac{Q_1}{3}.$$

If we have $Q_1 > 0$, then

$$\frac{dRe\lambda}{d\tau}\Big|_{\omega=\omega_0,\tau=\tau_0} = \frac{1}{\omega_0^2}Sign\left\{\frac{H(\mu)}{B_2^2 + B_1^2\omega_0^2}\right\} > 0\,. \tag{23}$$

Based on the above result, we write the following theorem.

Theorem 3 *Assume that Theorem 1 holds and if* $Q_1 > 0$, $Q_3 \geq 0$, $Q_1^2 - 3Q_2 \geq 0$, *then the equilibrium* E^* *is locally asymptotically stable for all* $\tau < \tau_0$, *unstable for* $\tau > \tau_0$ *and a Hopf bifurcation occurs at* $\tau = \tau_0$, *where*

$$\tau_0 = \frac{1}{\omega_0} \cos^{-1}\left[\frac{\omega_0 B_1(\omega_0^3 - \omega_0 A_2) + B_2(\omega_0^2 A_1 - A_3)}{\omega_0^2 B_1^2 + B_2^2}\right].$$

Appendix 5

Using normal form theory and the centre manifold theorem [50], we here determine the direction of the Hopf bifurcation and the properties of bifurcating periodic solutions. Throughout this section, we always assume that system (1) undergoes a Hopf bifurcation at the positive equilibrium E^* for $\tau = \tau_0$ and then $\pm i\omega_0$ are the corresponding purely imaginary roots of the characteristic equation.

Let $(x, y, z, w)^T = (G_e - G_e^*, I - I^*, G_i - G_i^*, C - C^*)^T$. Then, using the Taylor series expansion for system (1) at E^*, we obtain

$$\begin{aligned}
\dot{x} &= a_{11}x + a_{12}y + c_{11}x^2 + c_{12}xy,\\
\dot{y} &= a_{21}x + a_{22}y + a_{23}z + c_{21}x^2 + c_{22}xy + c_{23}yz + c_{24}z^2,\\
\dot{z} &= a_{31}x + a_{32}y(t-\tau) + a_{33}z + c_{31}x^2 + c_{32}xy(t-\tau),\\
\dot{w} &= a_{43}z + a_{44}w + c_{41}zw + c_{42}w^2.
\end{aligned} \tag{24}$$

Here, all a_{ij}'s are given in (15) and $c_{11} = -\frac{vk_1}{(k_1+G_e^*)^3} + \frac{rk_2I^*}{(k_2+G_e^*)^3}$, $c_{12} = \frac{rk_2}{(k_2+G_e^*)^2}$, $c_{21} = -\frac{ek_3I^*}{(k_3+G_e^*)^3}$, $c_{22} = \frac{ek_3}{(k_3+G_e^*)^2}$, $c_{23} = -\frac{sk_m}{(k_m+G_i^*)^2}$, $c_{24} = -\frac{sk_mI^*}{(k_m+G_i^*)^3}$, $c_{31} = -\frac{rk_2I^*}{(k_2+G_e^*)^3}$, $c_{32} = -c_{12}$, $c_{41} = -\frac{2nk_5^2C^*}{(k_5^2+C^{*2})^2}$, $c_{42} = \frac{pk_4^2(k_4^2-3C^{*2})}{(k_4^2+C^{*2})^3} - \frac{nk_5^2G_i^*(k_5^2-3C^{*2})}{(k_5^2+C^{*2})^3}$.

Now, let $\tau = \tau_0 + \mu$ and $u_t(\theta) = u(t+\theta)$ for $\theta \in [-\tau, 0]$. Denote $\mathbf{C}^k([-\tau, 0], \mathbb{R}^4) = \{\phi | \phi : [-\tau, 0] \to \mathbb{R}^4\}$, ϕ has $k-$th order continuous derivative. For the initial conditions $\phi(\theta) = (\phi_1(\theta), \phi_2(\theta), \phi_3(\theta), \phi_4(\theta))^T \in \mathbf{C}([-\tau, 0], \mathbb{R}^4)$, (24) can be written as

$$\dot{u}(t) = L_\mu(u_t) + F(u_t, \mu), \tag{25}$$

where $u(t) = (u_1(t), u_2(t), u_3(t), u_4(t))^T \in \mathbf{C}$, $L_\mu : \mathbf{C} \to \mathbb{R}^4$ and $F : \mathbf{C} \to \mathbb{R}^4$ are given, respectively, by

$$\begin{aligned}
L_\mu\phi &= (\tau_0 + \mu)M_1\phi(0) + (\tau_0 + \mu)M_2\phi(-\tau),\\
F(\phi, \mu) &= (\tau_0 + \mu)F.
\end{aligned} \tag{26}$$

Here L_μ is a one parameter family of bounded linear operators in $\mathbf{C}$, whereas M_1 and M_2 are given in (15) and

$$F = \begin{pmatrix} c_{11}\phi_1(0)\phi_1(0) + c_{12}\phi_1(0)\phi_2(0) \\ c_{21}\phi_1(0)\phi_1(0) + c_{22}\phi_1(0)\phi_2(0) + c_{23}\phi_2(0)\phi_3(0) + c_{24}\phi_3(0)\phi_3(0) \\ fc_{31}\phi_1(0)\phi_1(0) + c_{32}\phi_1(0)\phi_2(-\tau) \\ c_{41}\phi_3(0)\phi_4(0) + c_{42}\phi_4(0)\phi_4(0) \end{pmatrix}.$$

By the Reisz representation theorem, there exists a function $\eta(\theta, \mu)$ of bounded variation for $\theta \in [-\tau, 0]$ such that

$$L_\mu\phi = \int_{-\tau}^{0} d\eta(\theta, \mu)\phi(\theta). \tag{27}$$

We can choose

$$\eta(\theta, \mu) = (\tau_0 + \mu)M_1\delta(\theta) + (\tau_0 + \mu)M_2\delta(\theta + \tau), \tag{28}$$

where $\delta(\theta)$ is the Dirac delta function. For $\phi \in \mathbf{C}^1([-\tau, 0], \mathbb{R}^4)$, we define

$$A(\mu)\phi = \begin{cases} \frac{d\phi}{d\theta}, & \theta \in [-\tau, 0) \\ \int_{-\tau}^{0} d\eta(\theta, \mu)\phi(\theta), & \theta = 0, \end{cases} \tag{29}$$

$$R(\mu)\phi = \begin{cases} 0, & \theta \in [-\tau, 0) \\ F(\phi, \mu), & \theta = 0. \end{cases} \tag{30}$$

Since $\dot{u}(t) = \dot{u}_t(\theta)$, (25) can be written as

$$\dot{u}(t) = A(\mu)u_t + R(\mu)u_t, \tag{31}$$

where $u_t = u(t+\theta), \theta \in [-\tau, 0]$. For $\psi \in \mathbf{C}^1([0, \tau], \mathbb{R}^4)$, let us define the adjoint operator A^* of A as

$$A^*\psi(s)\phi = \begin{cases} \frac{d\psi(s)}{ds}, & s \in [-\tau, 0) \\ \int_{-\tau}^{0} d\eta(\theta, \mu)\phi(\theta), & s = 0. \end{cases} \tag{32}$$

For $\phi \in \mathbf{C}^1([-\tau, 0], \mathbb{R}^4)$ and $\psi \in \mathbf{C}^1([0, \tau], \mathbb{R}^4)$, in order to normalize the eigenvalues of operators A and A^*, we also define a bilinear inner product

$$< \psi, \phi >= \overline{\psi}(0)\phi(0) - \int_{\theta=-\tau}^{0} \int_{\xi=0}^{\theta} \overline{\psi}(\xi - \theta)(d\eta(\theta))\phi(\xi)d\xi, \tag{33}$$

where $\eta(\theta) = \eta(\theta, 0)$ and $\overline{\psi}$ is the complex conjugate of ψ. One can verify that A^* and $A(0)$ are adjoint operators with respect to this bilinear form.

We assume that $\pm i\omega_0$ are eigenvalues of $A(0)$ and the other eigenvalues have strictly negative parts. Thus, they are also eigenvalues of A^*. Now we compute the eigenvector q of A corresponding to the eigenvalue $i\omega_0$ and the eigenvector q^* of A^* corresponding to $-i\omega_0$. Suppose that $q(\theta) = (1, p_1, p_2, p_3)^T e^{i\omega_0\theta}$ is the eigenvector of $A(0)$ associated with $i\omega_0$, then $A(0)q(\theta) = i\omega q(\theta)$. From the definition of $A(0)$, (26), (27) and (29), we have

$$(M_1 + M_2 e^{-i\omega_0\tau_0} - I_4 i\omega_0)q(0) = \mathbf{0}. \tag{34}$$

Solving (34), we obtain $q(0) = (1, p_1, p_2, p_3)^T$, where $p_1 = \frac{i\omega_0 - a_{11}}{a_{12}}$, $p_2 = \frac{a_{12}a_{31} + a_{32}(i\omega_0 - a_{11})e^{-i\omega_0\tau_0}}{a_{12}(i\omega_0 - a_{33})}$, $p_3 = \frac{a_{43}(i\omega_0 - a_{11})(i\omega_0 - a_{22}) - a_{12}a_{21}a_{43}}{a_{12}a_{23}(i\omega_0 - a_{44})}$.

Similarly, let the eigenvector q^* of A^* corresponding to $-i\omega_0$ is $q^*(s) = (\frac{1}{D})(1, p_1^*, p_2^*, p_3^*)^T e^{i\omega_0 s}$, $s \in [0, \tau]$. Again, using the definition of A^* and (26), (27), (29), we get

$$({M_1}^T + {M_2}^T e^{-i\omega_0\tau_0} + I_4 i\omega_0)q^*(0) = \mathbf{0}. \tag{35}$$

Solving (35), one can obtain $q^*(0) = (\frac{1}{D})(1, p_1^*, p_2^*, p_3^*)^T$, where $p_1^* = \frac{a_{21}a_{31}e^{i\omega_0\tau_0} - a_{32}(a_{11} + i\omega_0)}{a_{21}a_{32} - a_{31}(a_{22} + i\omega_0)e^{i\omega_0\tau_0}}$, $p_2^* = \frac{a_{23}p_1^*}{a_{33} + i\omega_0}$, $p_3^* = 0$.

In order to assume that $< q^*, q >= 1$, we must determine the value of D. From (33), we get

$$\begin{aligned}
< q^*, q > &= \overline{q^*}^T(0)q(0) - \int_{\theta=-\tau_0}^{0}\int_{\xi=0}^{\theta}\overline{q^*}^T(\xi-\theta)(d\eta(\theta))Q(\xi)d\xi \\
&= \frac{1}{D}(1 + p_1\overline{p_1}^* + p_2\overline{p_2}^* + p_3\overline{p_3}^*) \\
&\quad - \int_{-\tau_0}^{0}\int_{0}^{\theta}\frac{1}{D}(1, \overline{p_1}^*, \overline{p_2}^*, \overline{p_3}^*)e^{-i\omega_0(\xi-\theta)} \\
&\quad \times(d\eta(\theta))(1, p_1, p_2, p_3)^T e^{i\omega_0\xi}d\xi \\
&= \frac{1}{D}(1 + p_1\overline{p_1}^* + p_2\overline{p_2}^* + p_3\overline{p_3}^*) - \int_{-\tau_0}^{0}\frac{1}{D}(1, \overline{p_1}^*, \overline{p_2}^*, \overline{p_3}^*)\theta e^{i\omega_0\theta} \\
&\quad \times(d\eta(\theta))(1, p_1, p_2, p_3)^T \\
&= \frac{1}{D}\Big[(1 + p_1\overline{p_1}^* + p_2\overline{p_2}^* + p_3\overline{p_3}^*) + \tau_0 e^{-i\omega_0\tau_0}(1, \overline{p_1}^*, \overline{p_2}^*, \overline{p_3}^*) \\
&\quad \times M(1, p_1, p_2, p_3)^T\Big] \\
&= \frac{1}{D}\Big[(1 + p_1\overline{p_1}^* + p_2\overline{p_2}^* + p_3\overline{p_3}^*) + \tau_0 e^{-i\omega_0\tau_0}\ p_1\overline{p_2}^* a_{32}\Big], \\
\overline{D} &= (1 + p_1\overline{p_1}^* + p_2\overline{p_2}^* + p_3\overline{p_3}^*) + \tau_0 e^{-i\omega_0\tau_0}\ p_1\overline{p_2}^* a_{32}. \qquad (36)
\end{aligned}$$

Let

$$\begin{aligned}
v(t) &= < q^*, u_t >, \\
W(t,\theta) &= u_t - vq - \overline{vq} = u_t - 2\Re(v(t)q(\theta)). \qquad (37)
\end{aligned}$$

On the centre manifold Ω_0, we have

$$W(t,\theta) = W(v(t), \overline{v}(t), \theta), \qquad (38)$$

where

$$W(v(t), \overline{v}(t), \theta) = W_{20}(\theta)\frac{v^2}{2} + W_{11}(\theta)v\overline{v} + W_{02}(\theta)\frac{\overline{v}^2}{2} + \cdots, \qquad (39)$$

v and $\overline{v}$ are local coordinates of the centre manifold Ω_0 in the direction of q^* and $\overline{q}^*$, respectively. Note that u_t real implies W is real. Considering only the real solutions, from (37), we obtain

$$\begin{aligned}
< q^*, W > &= < q^*, u_t - vq - \overline{vq} > \\
&= < q^*, u_t > -v(t) < q^*, q > -\overline{v}(t) < q^*, \overline{q} > . \qquad (40)
\end{aligned}$$

For the solution $u_t \in \Omega_0$ of (25), from (30) and (33), since $\mu = 0$, we have

$$\begin{aligned}
\dot{v}(t) &= < q^*, u_t > \\
&= < q^*, A(0)u_t + R(0)u_t > \\
&= < q^*, A(0)u_t > + < q^*, R(0)u_t > \\
&= < A^*q^*, u_t > + \overline{q^*}^T(0)F(u_t, 0) \\
&= i\omega_0 v(t) + \overline{q^*}^T(0)f_0(v, \overline{v}) \\
\dot{v}(t) &= i\omega_0 v(t) + g(v, \overline{v}), \qquad (41)
\end{aligned}$$

where

$$\begin{aligned} g(v,\overline{v}) &= \overline{q^*}^T(0) f_0 \\ &= \overline{q^*}^T(0) F(W(v,\overline{v},\theta) + 2\Re\{v(t)q(\theta),0\}) \\ &= g_{20}\frac{v^2}{2} + g_{11}v\overline{v} + g_{02}\frac{\overline{v}^2}{2} + g_{02}\frac{\overline{v}v^2}{2} + \cdots . \end{aligned} \tag{42}$$

Substituting (31) and (41) into (37), we get

$$\begin{aligned} \dot{W} &= \dot{u}(t) - \dot{v}q - \dot{\overline{v}}\,\overline{q} \\ &= Au_t + Ru_t - \left(i\omega_0 v + \overline{q^*}^T(0) f_0(v,\overline{v})\right) q - \left(i\omega_0\overline{v} + \overline{q^*}^T(0)\overline{f_0(v,\overline{v})}\right)\overline{q} \\ &= Au_t + Ru_t - Avq - A\overline{v}\,\overline{q} - 2\Re\left(\overline{q^*}^T(0) f_0(v,\overline{v})q\right). \end{aligned} \tag{43}$$

Now

$$\dot{W} = \begin{cases} AW - 2\Re\left(\overline{q^*}^T(0) f_0(v,\overline{v})q\right), & \theta \in [-\tau, 0) \\ AW - 2\Re\left(\overline{q^*}^T(0) f_0(v,\overline{v})q\right) + f_0(v,\overline{v}), & \theta = 0, \end{cases} \tag{44}$$

This can be written as

$$\dot{W} = AW + H(v,\overline{v},\theta), \tag{45}$$

where

$$H(v,\overline{v},\theta) = H_{20}(\theta)\frac{v^2}{2} + W_{11}(\theta)v\overline{v} + W_{02}(\theta)\frac{\overline{v}^2}{2} + \cdots . \tag{46}$$

On the centre manifold Ω_0, we have

$$\dot{W} = W_v\dot{v} + W_{\overline{v}}\dot{\overline{v}}. \tag{47}$$

Substituting (39) and (41) into (47), we get

$$\dot{W} = (W_{20}v + W_{11}\overline{v} + \cdots)(i\omega_0 v + g) + (W_{11}v + W_{02}\overline{v} + \cdots)(-i\omega_0\overline{v} + \overline{g}). \tag{48}$$

Again, substituting (39) and (46) into (45), we have

$$\dot{W} = (AW_{20} + H_{20})\frac{v^2}{2} + (AW_{11} + H_{11})v\overline{v} + (AW_{02} + H_{02})\frac{\overline{v}^2}{2} + \cdots . \tag{49}$$

Comparison of (48) and (49) gives

$$\begin{aligned} (A - 2i\omega_0)W_{20}(\theta) &= -H_{20}(\theta), \\ AW_{11}(\theta) &= -H_{11}(\theta), \\ (A + 2i\omega_0)W_{02}(\theta) &= -H_{02}(\theta). \end{aligned} \tag{50}$$

Since $u_t = u(t+\theta) = W(v,\overline{v},\theta) + vq + \overline{v}\,q$, we have

$$u_t = \begin{pmatrix} u_1(t+\theta) \\ u_2(t+\theta) \\ u_3(t+\theta) \\ u_4(t+\theta) \end{pmatrix} = \begin{pmatrix} W^{(1)}(v,\overline{v},\theta) \\ W^{(2)}(v,\overline{v},\theta) \\ W^{(3)}(v,\overline{v},\theta) \\ W^{(4)}(v,\overline{v},\theta) \end{pmatrix} + v\begin{pmatrix} 1 \\ p_1 \\ p_2 \\ p_3 \end{pmatrix} e^{i\omega_0\theta} + \overline{v}\begin{pmatrix} 1 \\ \overline{p}_1 \\ \overline{p}_2 \\ \overline{p}_3 \end{pmatrix} e^{-i\omega_0\theta}. \tag{51}$$

This gives

$$\begin{aligned} u_j(t+\theta) &= \left(W_{20}^{(j)}(\theta)\frac{v^2}{2} + W_{11}^{(j)}(\theta)v\overline{v} + W_{02}^{(j)}(\theta)\frac{\overline{v}v^2}{2} + \cdots\right) \\ &\quad + vp_j e^{i\omega_0\theta} + \overline{v}\,\overline{p}_j e^{-i\omega_0\theta}, \end{aligned} \tag{52}$$

where $j = 1, 2, 3, 4$, and $p_0 = \overline{p}_0 = 1$.

It can be observed that

$$\phi_j(0) = vp_j + \overline{v}\,\overline{p}_j + W_{20}^{(j)}(0)\frac{v^2}{2} + W_{11}^{(j)}(0)v\overline{v} + W_{02}^{(j)}(0)\frac{\overline{v}v^2}{2} + \cdots, \tag{53}$$

where $j = 1, 2, 3, 4$, and $p_0 = \overline{p}_0 = 1$ and

$$\begin{aligned}\phi_2(-\tau) = {} & vp_1e^{-i\omega_0\tau} + \overline{v}\,\overline{p}_1e^{i\omega_0\tau} + W_{20}^{(2)}(-\tau)\frac{v^2}{2} + W_{11}^{(2)}(-\tau)v\overline{v} \\ & + W_{02}^{(2)}(-\tau)\frac{\overline{v}v^2}{2} + \cdots\end{aligned} \tag{54}$$

From (41), it follows that

$$f_0(v,\overline{v}) = F = \left(\, F_{ij} \,\right)_{4\times 4}(v^2, \overline{v}^2, v\overline{v}, v^2\overline{v})^T, \tag{55}$$

where

$$\begin{aligned}
F_{11} &= c_{11} + c_{12}p_1, \quad F_{12} = c_{11} + c_{12}\overline{p_1}, \quad F_{13} = 2c_{11} + c_{12}\,(p_1 + \overline{p_1}), \\
F_{14} &= \left(c_{11} + \frac{1}{2}c_{12}\overline{p_1}\right) W_{20}^{(1)}(0) + (2c_{11} + c_{12}p_1)\, W_{11}^{(1)}(0) + c_{12}\left(W_{11}^{(2)}(0) + \frac{1}{2}W_{20}^{(2)}(0)\right), \\
F_{21} &= c_{21} + c_{22}p_1 + c_{23}p_1p_2 + c_{24}p_2^2, \quad F_{22} = c_{21} + c_{22}\overline{p_1} + c_{23}\overline{p_1p_2}, \\
F_{23} &= 2c_{21} + c_{22}\,(p_1 + \overline{p_1}) + c_{23}\,(p_1\overline{p_2} + p_2\overline{p_1}) + 2c_{24}p_2\overline{p_2}, \\
F_{24} &= \left(c_{21} + \frac{1}{2}c_{22}\overline{p_1}\right) W_{20}^{(1)}(0) + \frac{1}{2}\,(c_{22} + c_{23}\overline{p_2})\, W_{20}^{(2)}(0) + \left(\frac{1}{2}c_{23}\overline{p_1} + c_{24}\overline{p_2}\right) W_{20}^{(3)}(0) \\
&\quad + (2c_{21} + c_{22}p_1)\, W_{11}^{(1)}(0) + (c_{22} + c_{23}p_2)\, W_{11}^{(2)}(0) + (c_{23}p_1 + 2c_{24}p_2)\, W_{11}^{(3)}(0), \\
F_{31} &= c_{31} + c_{32}p_1e^{-i\omega_0\tau}, \quad F_{32} = c_{31} + c_{32}\overline{p_1}e^{i\omega_0\tau}, \\
F_{33} &= 2c_{31} + c_{32}\left(p_1e^{-i\omega_0\tau} + \overline{p_1}e^{i\omega_0\tau}\right), \\
F_{34} &= \left(c_{31} + \frac{1}{2}c_{32}\overline{p_1}e^{i\omega_0\tau}\right) W_{20}^{(1)}(0) + c_{32}\left(\frac{1}{2}W_{20}^{(2)}(-\tau) + W_{11}^{(2)}(-\tau)\right) \\
&\quad + \left(2c_{31} + c_{32}p_1e^{-i\omega_0\tau}\right) W_{11}^{(1)}(0), \\
F_{41} &= c_{42}p_3^2 + c_{41}p_2p_3, \quad F_{42} = c_{42}\overline{p_3}^2 + c_{41}\overline{p_2p_3}, \\
F_{43} &= 2c_{42}p_3\overline{p_3} + c_{41}\,(\overline{p_2}p_3 + p_2\overline{p_3}), \\
F_{44} &= \left(c_{42}\overline{p_3} + \frac{1}{2}c_{41}\overline{p_2}\right) W_{20}^{(4)}(0) + (2c_{42}p_3 + c_{41}p_2)\, W_{11}^{(4)}(0) \\
&\quad + c_{41}\left(p_3W_{11}^{(3)}(0) + \frac{1}{2}\overline{p_3}W_{20}^{(3)}(0)\right).
\end{aligned}$$

Since $\overline{q}^*(0) = \frac{1}{\overline{D}}(1, \overline{p_1}^*, \overline{p_2}^*, \overline{p_3}^*)^T$, we have

$$\begin{aligned}
g(v,\overline{v}) &= \overline{q^*}^T(0)\, f_0(v,\overline{v}) \\
&= \frac{1}{\overline{D}}(1, \overline{p_1}^*, \overline{p_2}^*, \overline{p_3}^*)\left(\, F_{ij} \,\right)_{4\times 4}(v^2, \overline{v}^2, v\overline{v}, v^2\overline{v})^T \\
&= \frac{1}{2}\left(g_{20}v^2 + g_{02}\overline{v}^2 + 2g_{11}v\overline{v} + g_{21}v^2\overline{v}\right),
\end{aligned} \tag{56}$$

where

$$
\begin{aligned}
g_{20} &= \frac{2}{D}\left(F_{11}+F_{21}\overline{p_1}^{*}+F_{31}\overline{p_2}^{*}+F_{41}\overline{p_3}^{*}\right),\\
g_{02} &= \frac{2}{D}\left(F_{12}+F_{22}\overline{p_1}^{*}+F_{32}\overline{p_2}^{*}+F_{42}\overline{p_3}^{*}\right),\\
g_{11} &= \frac{1}{D}\left(F_{13}+F_{23}\overline{p_1}^{*}+F_{33}\overline{p_2}^{*}+F_{43}\overline{p_3}^{*}\right),\\
g_{21} &= \frac{2}{D}\left(F_{14}+F_{24}\overline{p_1}^{*}+F_{34}\overline{p_2}^{*}+F_{44}\overline{p_3}^{*}\right).
\end{aligned}
\tag{57}
$$

From (48) and (49), we get

$$
\begin{aligned}
H(v,\overline{v},\theta) &= -2\,\mathrm{Re}\,\left(\overline{q^{*}}^{T}(0)\,f_0(v,\overline{v})q(\theta)\right)\\
&= -2\,\mathrm{Re}\,\left(g(v,\overline{v})q(\theta)\right)\\
&= -g(v,\overline{v})q(\theta)-\overline{g}(v,\overline{v})\overline{q}(\theta)\\
&= -\frac{1}{2}\left(g_{20}v^2+g_{02}\overline{v}^2+2g_{11}v\overline{v}+g_{21}v^2\overline{v}\right)q(\theta)\\
&\quad -\frac{1}{2}\left(\overline{g}_{20}\overline{v}^2+\overline{g}_{02}v^2+2\overline{g}_{11}v\overline{v}+\overline{g}_{21}\overline{v}^2v\right)\overline{q}(\theta).
\end{aligned}
\tag{58}
$$

Comparing with (46), we have

$$
\begin{aligned}
H_{20}(\theta) &= -g_{20}q(\theta)-\overline{g}_{02}\overline{q}(\theta),\\
H_{11}(\theta) &= -g_{11}q(\theta)-\overline{g}_{11}\overline{q}(\theta),\\
H_{02}(\theta) &= -g_{02}q(\theta)-\overline{g}_{20}\overline{q}(\theta).
\end{aligned}
\tag{59}
$$

It follows from (29) and (50) that

$$
\begin{aligned}
\dot{W}(\theta) &= AW_{20} = 2i\omega_0W_{20}(\theta)-H_{20}(\theta)\\
&= 2i\omega_0W_{20}+g_{20}q(0)e^{i\omega_0\theta}+\overline{g}_{02}\overline{q}(0)e^{-i\omega_0\theta}.
\end{aligned}
\tag{60}
$$

Solving for $W_{20}(\theta)$ and $W_{11}(\theta)$ from above equation, one gets

$$
\begin{aligned}
W_{20}(\theta) &= \frac{ig_{20}}{\omega_0}q(0)e^{i\omega_0\theta}+\frac{i\overline{g}_{02}}{3\omega_0}q(0)e^{-i\omega_0\theta}+E_1e^{2i\omega_0\theta},\\
W_{11}(\theta) &= -\frac{ig_{11}}{\omega_0}q(0)e^{i\omega_0\theta}+\frac{i\overline{g}_{11}}{\omega_0}q(0)e^{-i\omega_0\theta}+E_2,
\end{aligned}
\tag{61}
$$

where E_1 and E_2 can be determined by setting $\theta=0$ in $H(v,\overline{v},\theta)$. In fact, we have

$$
\begin{aligned}
H(v,\overline{v},0) &= -2\,\mathrm{Re}\,\left(\overline{q^{*}}^{T}(0)\,f_0(v,\overline{v})q(0)\right)+f_0(v,\overline{v})\\
&= -\frac{1}{2}\left(g_{20}v^2+g_{02}\overline{v}^2+2g_{11}v\overline{v}+g_{21}v^2\overline{v}\right)q(0)\\
&\quad -\frac{1}{2}\left(\overline{g}_{20}\overline{v}^2+\overline{g}_{02}v^2+2\overline{g}_{11}v\overline{v}+\overline{g}_{21}\overline{v}^2v\right)\overline{q}(0)\\
&\qquad +\left(F_{ij}\right)_{4\times4}(v^2,\overline{v}^2,v\overline{v},v^2\overline{v})^T.
\end{aligned}
\tag{62}
$$

Comparing the coefficients of the above equations with those in (47), it follows that

$$
\begin{aligned}
H_{20}(0) &= -g_{20}q(0)-\overline{g}_{02}\overline{q}(0)+(F_{11},F_{21},F_{31},F_{41})^T,\\
H_{11}(0) &= -g_{11}q(0)-\overline{g}_{11}\overline{q}(0)+(F_{13},F_{23},F_{33},F_{43})^T.
\end{aligned}
\tag{63}
$$

By the definition of A and (30) and (50), we get

$$\begin{aligned}\int_{-\tau_0}^{0} d\eta(\theta) W_{20}(\theta) &= AW_{20} = 2i\omega_0 W_{20}(0) - H_{20}(0),\\ \int_{-\tau_0}^{0} d\eta(\theta) W_{11}(\theta) &= AW_{11} = -H_{11}(0).\end{aligned} \tag{64}$$

One can notice that

$$\begin{aligned}\left[i\omega_0 I_4 - \int_{-\tau_0}^{0} e^{i\omega_0\theta} d\eta(\theta)\right] q(0) = 0,\\ \left[-i\omega_0 I_4 - \int_{-\tau_0}^{0} e^{-i\omega_0\theta} d\eta(\theta)\right] \overline{q}(0) = 0.\end{aligned} \tag{65}$$

Thus, we obtain

$$\begin{aligned}\left[2i\omega_0 I_4 - \int_{-\tau_0}^{0} e^{2i\omega_0\theta} d\eta(\theta)\right] E_1 = (F_{11}, F_{21}, F_{31}, F_{41})^T,\\ \left[\int_{-\tau_0}^{0} d\eta(\theta)\right] E_2 = -(F_{13}, F_{23}, F_{33}, F_{43})^T,\end{aligned} \tag{66}$$

where $E_1 = (E_1^{(1)}, E_1^{(2)}, E_1^{(3)}, E_1^{(4)})^T$, $E_2 = (E_2^{(1)}, E_2^{(2)}, E_2^{(3)}, E_2^{(4)})^T$.

The above equation can be written as

$$\begin{aligned}(2i\omega_0 I_4 - M_1 - M_2 e^{-i\omega_0\tau_0} - I_4 i\omega_0) E_1 = (F_{11}, F_{21}, F_{31}, F_{41})^T,\\ (M_1 + M_2) E_2 = (F_{13}, F_{23}, F_{33}, F_{43})^T.\end{aligned} \tag{67}$$

From (61) and (67), we can calculate g_{21}, and we can derive the following parameters:

$$\begin{aligned}C_1(0) &= \frac{i}{2\omega_0}\left[g_{20}g_{11} - 2|g_{11}|^2 - \frac{1}{3}|g_{02}|^2\right] + \frac{g_{21}}{2},\\ \mu_2 &= -\frac{\mathrm{Re}\,(C_1(0))}{\mathrm{Re}\,(\lambda'(\tau_0))},\\ \beta_2 &= 2\,\mathrm{Re}\,(C_1(0)),\\ T_2 &= -\frac{\mathrm{Im}\,(C_1(0)) + \mu_2\,\mathrm{Im}\,(\lambda(\tau_0))}{\omega_0}.\end{aligned} \tag{68}$$

Thus, we have the following results:

Theorem 4 *The periodic solution is supercritical (subcritical) if $\mu_2 > 0$ ($\mu_2 < 0$), the bifurcating periodic solutions are orbitally asymptotically stable (unstable) if $\beta_2 < 0$ ($\beta_2 > 0$), the period of the bifurcating periodic solution increases (decreases) if $T_2 > 0$ ($T_2 < 0$).*

References

1. Bers, D.M.: Cardiac excitation-contraction coupling. Nature **415**(6868), 198–205 (2002)
2. Dupont, G., Combettes, L., Bird, G.S., Putney, J.W.: Calcium oscillations. Cold Spring Harb. Perspect. Biol. 3, 3 a004226 (2011)
3. Taylor, J.A., Lipsitz, L.A.: Heart rate variability standards. Circulation **95**(1), 280–281 (1997)
4. Tang, Y., Stephenson, J.L., Othmer, H.G.: Simplification and analysis of models of calcium dynamics based on IP3-sensitive calcium channel kinetics. Biophys. J. **70**(1), 246–263 (2006)

5. Santos, R.M., Rosario, L.M., Nadal, A., Garcia-Sancho, J., Soria, B., Valdeolmillos, M.: Widespread synchronous Ca^{2+} oscillations due to bursting electrical activity in single pancreatic islets. Pflugers Arch. **418**, 417–422 (1991)
6. Gilon, P., Shepherd, R.M., Henquin, J.C.: Oscillations of secretion driven by oscillations of cytoplasmic Ca^{2+} as evidenced in single pancreatic islets. J. Biol. Chem. **268**, 22265–22268 (1993)
7. Bertram, R., Sherman, A., Satin, L.S.: Electrical bursting, calcium oscillations, and synchronization of pancreatic islets. Adv. Exp. Med. Biol. **654**, 261–279 (2010)
8. Makroglou, A., Li, J., Kuang, Y.: Mathematical models and software tools for the glucose-insulin regulatory system and diabetes: an overview. Appl. Numer. Math. **56**(3-4), 559–573 (2006)
9. Liu, Y.J., Tengholm, A., Grapengiesser, E., Hellman, B., Gylfe, E.: Origin of slow and fast oscillations of Ca^{2+} in mouse pancreatic islets. J. Physiol. **508**(2), 471–481 (1998)
10. Wu, Z., Chui, C.K., Hong, G.S., Chang, S.: Physiological analysis on oscillatory behavior of glucose–insulin regulation by model with delays. J. Theor. Biol. **280**(1), 1–9 (2011)
11. Bairagi, N., Chatterjee, S., Chattopadhyay, J.: Variability in the secretion of CRH, ACTH & cortisol and understandability of the HPA axis dynamics – a mathematical study based on clinical evidences. Math. Med. Biol. **25**(1), 37–63 (2008)
12. Landstrom, A.P., Dobrev, D., Wehrens, X.H.T.: Calcium signaling and cardiac arrhythmias. Circ. Res. **120**, 1969–1993 (2017)
13. Maack, C., O'Rourke, B.: Excitation-contraction coupling and mitochondrial energetics. Basic Res. Cardiol. **102**(5), 369–392 (2007)
14. Shao, D., Tian, R.: Glucose transporters in cardiac metabolism and hypertrophy. Comprehensive Physiology **6**(1), 331 (2015)
15. Montessuit, C., Lerch, R.: Regulation and dysregulation of glucose transport in cardiomyocytes. Biochim. Biophys. Acta **1833**(4), 848–856 (2013)
16. Satoh, T.: Molecular mechanisms for the regulation of insulin-stimulated glucose uptake by small guanosine triphosphatases in skeletal muscle and adipocytes. Int. J. Mol. Sci. **15**, 18677–18692 (2014)
17. Belke, D.D., Betuing, S., Tuttle, M.J., Graveleau, C., Young, M.E., Pham, M., Zhang, D., Cooksey, R.C., McClain, D.A., Litwin, S.E., Taegtmeyer, H.: Insulin signaling coordinately regulates cardiac size, metabolism, and contractile protein isoform expression. J. Clin. Invest. **109**(5), 629–639 (2002)
18. Wright, J.J., Kim, J., Buchanan, J., Boudina, S., Sena, S., Bakirtzi, K., Ilkun, O., Theobald, H.A., Cooksey, R.C., Kandror, K.V., Abel, E.D.: Mechanisms for increased myocardial fatty acid utilization following short-term high-fat feeding. Cardiovasc. Res. **82**, 351–360 (2009)
19. Ormazabal, V., Nair, S., Elfeky, O., Aguayo, C., Salomon, C., Zuñiga, F.A.: Association between insulin resistance and the development of cardiovascular disease. Cardiovasc. Diabetol. **17**(1), 122 (2018)
20. Ren, J., Gintant, G.A., Miller, R.E., Davidoff, A.J.: High extracellular glucose impairs cardiac EC coupling in a glycosylation-dependent manner. Am. J. Physiol. (Heart Circ.) **273**(6), H2876–H2883 (1997)
21. Ramirez-Correa, G.A., Ma, J., Slawson, C., Zeidan, Q., Lugo-Fagundo, N.S., Xu, M., Shen, X., Gao, W.D., Caceres, V., Chakir, K., DeVine, L.: Removal of abnormal myofilament O-GlcNAcylation restores $Ca^{2}+$ sensitivity in diabetic cardiac muscle. Diabetes **64**, 3573–3587 (2015)
22. Makroglou, A., Li, J., Kuang, Y.: Mathematical models and software tools for the glucose-insulin regulatory system and diabetes: An overview. Appl. Numer. Math **56**, 559–573 (2006)
23. Bertrand, L., Horman, S., Beauloye, C., Vanoverschelde, J.L.: Insulin signalling in the heart. Cardiovasc. Res. **79**, 238–248 (2008)
24. Bryant, N., Govers, J.N., James, D.E.: Regulated transport of the glucose transporter GLUT4. Nature Rev. Mol. Cell Bio. **3**, 267–277 (2002)
25. Wilson, J.E.: Isozymes of mammalian hexokinase: structure, subcellular localization and metabolic function. J. Exp. Biology **206**(12), 2049–2057 (2003)
26. Piquereau, J., Novotova, M., Fortin, D., Garnier, A., Ventura-Clapier, R., Veksler, V., Joubert, F.: Postnatal development of mouse heart: formation of energetic microdomains. J. Physiol. **588**(13), 2443–2454 (2010)
27. Dupont, G., Falcke, M., Kirk, V., Sneyd, J.: Models of Calcium Signalling, p. 43. Springer International Publishing, Cham (2016)
28. Freckmann, G., Hagenlocher, S., Baumstark, A., Jendrike, N., Gillen, R.C., Rössner, K., Haug, C.: Continuous glucose profiles in healthy subjects under everyday life conditions and after different meals. J. Diabetes Sci. Technol. **1**(5), 695–703 (2007)
29. Aronoff, S.L., Berkowitz, K., Shreiner, B., Want, L.: Glucose metabolism and regulation: beyond insulin and glucagon. Diabetes Spectrum **17**(3), 183–190 (2004)
30. Saltiel, A.R., Kahn, C.R.: Insulin signalling and the regulation of glucose and lipid metabolism. Nature **414**(6865), 799–806 (2001)

31. Shen, P., Larter, R.: Chaos in intracellular Ca^{2+} oscillations in a new model for non-excitable cells. Cell Calcium **17**, 225–232 (1995)
32. Houart, G., Dupont, G., Goldbeter, A.: Bursting, chaos and birhythmicity originating from self-modulation of the inositol 1,4,5-trisphosphate signal in a model for intracellular Ca^{2+} oscillations. Bull. Math. Biology **61**, 507–530 (1999)
33. Boutayeb, W., Lamlili, M., Boutayeb, A., Derouich, M.: Mathematical modelling and simulation of β-cell mass, insulin and glucose dynamics: effect of genetic predisposition to diabetes. J. Biomed. Sci. Eng. Sci. Res. Publ. **7**(06), 330–342 (2014)
34. Kummer, U., Olsen, L.F., Dixon, C.J., Green, A.K., Bornberg-Bauer, E., Baier, G.: Switching from simple to complex oscillations in calcium signaling. Biophys. J. **79**, 1188–1195 (2000)
35. Das, P.N., Mehrotra, P., Mishra, A., Bairagi, N., Chatterjee, S.: Calcium dynamics in cardiac excitatory and non-excitatory cells and the role of gap junction. Math. Biosci. **289**, 51–68 (2017)
36. Das, P.N., Pedruzzi, G., Bairagi, N., Chatterjee, S.: Coupling calcium dynamics and mitochondrial bioenergetic: an in silico study to simulate cardiomyocyte dysfunction. Mol. BioSyst. **12**(3), 806–817 (2016)
37. Holten, M.K., Zacho, M., Gaster, M., Juel, C., Wojtaszewski, J.F., Dela, F.: Strength training increases insulin-mediated glucose uptake, GLUT4 content, and insulin signaling in skeletal muscle in patients with type 2 diabetes. Diabetes **53**(2), 294–305 (2004)
38. Rose, A.J., Richter, E.A.: Skeletal muscle glucose uptake during exercise: how is it regulated? Physiology **20**(4), 260–270 (2005)
39. Engelgau, M.M., Narayan, K.M., Herman, W.H.: Screening for type 2 diabetes. Clinical Diabetes **23**(10), 1563–80 (2000)
40. Melmed, S., Polonsky, K.S., Larsen, P.R., Kronenberg, H.M.: Williams Textbook of Endocrinology. Elsevier Health Sciences (2015)
41. Swillens, S., Mercan, D.: Computer simulation of a cytosolic calcium oscillator. Biochem. J. **271**(3), 835–838 (1990)
42. Blower, S.M., Dowlatabadi, H.: Sensitivity and uncertainty analysis of complex829 models of disease transmission: an HIV model, as an example. Int. Stat. Rev. **62**, 229–243 (1994)
43. Pedruzzi, G., Rao, K.V.S., Chatterjee, S.: Mathematical model of mycobacterium-host interaction describes physiology of persistence. J. Theor. Biol. **376**, 105–117 (2015)
44. Domenighetti, A.A., Danes, V.R., Curl, C.L., Favaloro, J.M., Proietto, J., Delbridge, L.M.D.: Targeted GLUT-4 deficiency in the heart induces cardiomyocyte hypertrophy and impaired contractility linked with Ca^{2+} and proton flux dysregulation. J. Mol. Cell. Cardiol. **48**(4), 663–672 (2010)
45. Fauconnier, J., Lanner, J.T., Zhang, S.J., Tavi, P., Bruton, J.D., Katz, A., Westerblad, H.: Insulin and inositol 1,4,5-triphosphate trigger abnormal cytosolic Ca^{2+} transients and reveal mitochondrial Ca^{2+} handling defects in cardiomyocytes of ob/ob mice. Diabetes **54**, 2375–2381 (2005)
46. Knipl, D.H.: Fundamental properties of differential equations with dynamically defined delayed feedback. Electron. J. Qual. Theory Differ. Equ. **17**, 1–18 (2013)
47. Birkhoff, G., Rota, G.C.: Ordinary Differential Equations. Wiley, New York (1978)
48. Yang, J.Y., Wang, X.Y., Li, X.Z.: Hopf bifurcation for a model of HIV infection of T cells with virus released delay. Discrete Dyn. Nat. Soc. **2011**, 649650 (2011)
49. Song, Y., Han, M., Wei, J.: Stability and Hopf bifurcation analysis on a simplified BAM neural network with delays. Physica D **200**(3-4), 185–204 (2005)
50. Hassard, B.D., Kazarinoff, N.D., Wan, Y.H.: Theory and applications of Hopf bifurcation. vol. 41 of London Mathematical Society Lecture Note Series. Cambridge University Press, Cambridge (1981)